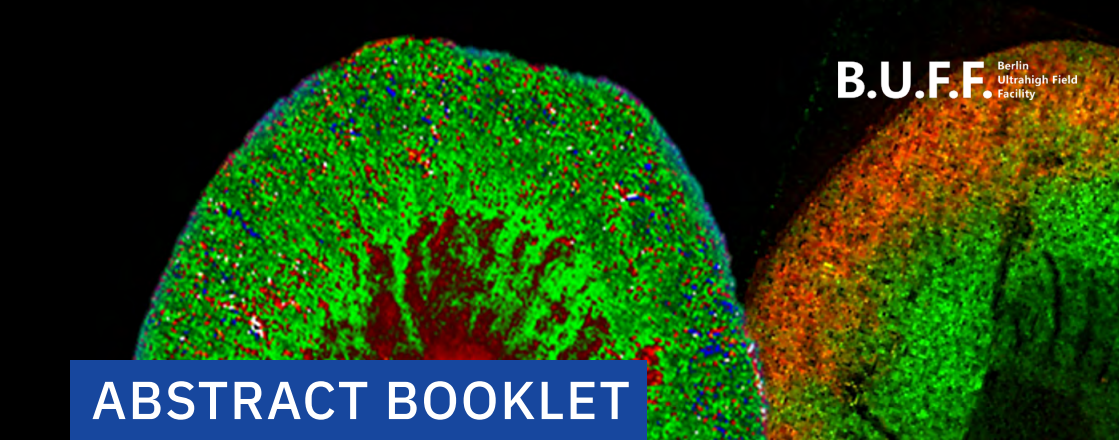

B.U.F.F. Berlin Ultrahigh Field Facility

ABSTRACT BOOKLET

14. ANNUAL SCIENTIFIC SYMPOSIUM

Ultrahigh Field Magnetic Resonance: Clinical Needs, Research Promises and Technical Solutions

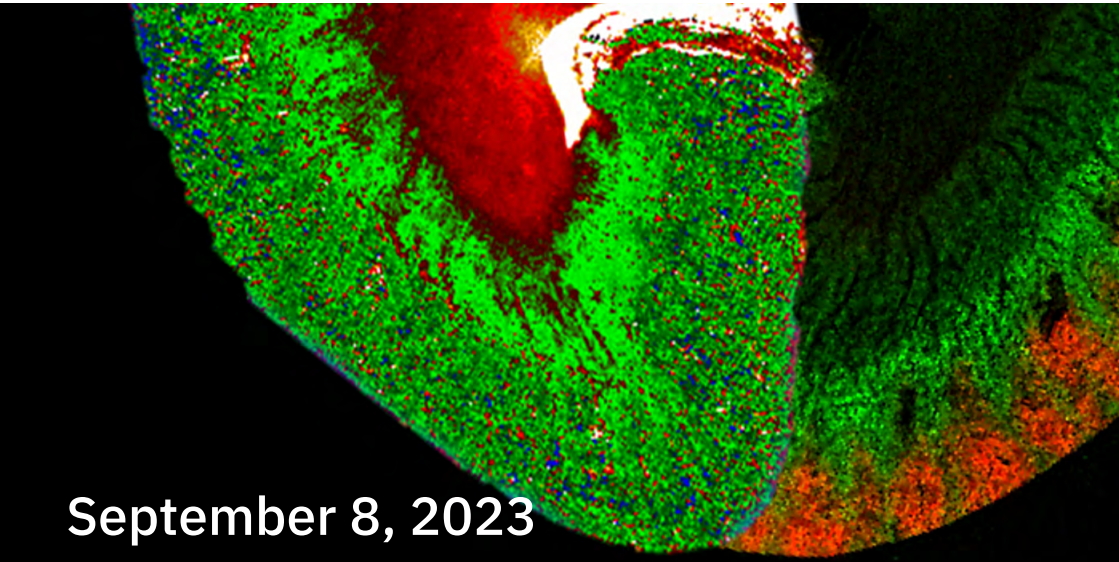

September 8, 2023

8:15 am - 6:00 pm

Max Delbrück Communications Center (MDC.C)

MAX DELBRÜCK CENTER

www.mdc-berlin.de

www.mdc-berlin.de/MRSymposium2023

Max Delbrück Center for Molecular Medicine
in the Helmholtz Association

Robert-Rössle-Straße 10, 13125 Berlin, Germany

Message from the organizers

Dear colleagues and friends,

Very warm welcome to Berlin. It is time to ride the wave of ultrahigh field MRI again.

We are most of all excited by the larger audience that has joined us for the **14th Scientific Symposium on Clinical Needs, Research Promises and Technical Solutions in Ultrahigh Field Magnetic Resonance**. It is a hybrid experience that combines our established in-person meeting and setup with a virtual meeting in favour of changing scientific communication and exchange for the better.

Imaging bridges, a crucial gap in space and time in life science and medicine: from atomic to anatomic objects to whole body imaging, from picoseconds to years in population studies. New molecular and cellular insights are obtained from imaging. These findings should be integrated with data science into a coherent picture of tissues, organs and organisms for early interception of disease. These fundamental developments call for hitherto unavailable research frameworks, international partnership and collaborative culture to promote strong ties across multiple research domains and imaging modalities; connecting nanoscopic views, length scales, time scales and mesoscopic pictures with mechanistic insights and macroscopic function of biological and clinical importance.

To meet this goal the Max Delbrück Center for Molecular Medicine; the Weizmann Institute of Science in Rehovot, Israel; the Humboldt University of Berlin and the Charité - Universitätsmedizin Berlin have joined forces in the Helmholtz International Research School (HIRS) on imaging from the **NA**no to the **ME**so *(iNAMES, https://www.mdc-berlin.de/inames)*. These efforts are complemented by the **H**elmholtz **I**maging **P**latform (HIP), with the Max Delbrück Center being a HIP core in collaboration with the DESY Hamburg and DKFZ Heidelberg. iNAMES and HIP are acting as springboards to intensify scientific interactions in imaging, data sciences, information technologies and digital engineering research fields.

The field of Magnetic Resonance (MR) has evolved rapidly over the past quarter of a century, allowing for an ever growing number of applications across a broad spectrum of basic, translational and clinical research. One important development which is in the spotlight of MR research is Ultrahigh Field Magnetic Resonance (UHF-MR). The pace of discovery is heartening and a powerful motivator to transfer the lessons learned at ultrahigh fields from basic research into the clinical scenario. These efforts are fueled by the unmet clinical needs and the quest for advancing the capabilities of diagnostic MR imaging – today.

Message from the organizers

The development of UHF-MR is moving forward at an amazing speed that is breaking through technical barriers almost as fast as they appear. UHF-MR has become an engine for innovation in experimental and clinical research. The reasons for moving UHF-MR into clinical applications are more compelling than ever. Images from these instruments have revealed new aspects of the anatomy, functions and physio-metabolic characteristics of the brain, heart, joints, kidneys, liver, eye, and other organs/tissues, at an unparalleled quality. UHF-MR has a staggering number of potential uses in neuroscience, neurology, radiology, neuroradiology, cardiology, internal medicine, oncology, nephrology, ophthalmology and other related clinical fields. As they are developed, we will push the boundaries of MR physics, biomedical engineering and biomedical sciences in many other ways.

With 7.0 T human MRI now widely used in clinical research, there is increasing interest in exploring even higher magnetic field strengths. This includes pioneering reports on MRI technology at 9.4 T, 10.5 T and 11.7 T and corresponding in vivo applications. The MR research and superconductor science community have already taken even more ambitious steps towards the future, envisioning human MR at 14.0 T. Recently, the Dutch National 14 Tesla Initiative in Medical Science received funding for the implementation of the first 14.0 T class human MR instrument. Joint efforts of the nuclear magnetic resonance (NMR) and MRI communities identified the scientific question that drives these ambitions, together with the technological challenges and prospects for achieving human MRI at 20.0 T. These bold steps will require rigorous technical developments, assessment of physiological constraints and in vivo evaluation studies, that have to be tested and validated by those who adopt the technology. The symposium offers ample opportunity for discussion and exchange on how such efforts can lead to valuable results.

Realizing these opportunities, we are very much delighted to very warm welcome you at the 14th Annual Scientific Symposium on Clinical Needs, Research Promises and Technical Solutions in Ultrahigh Field MR. The symposium is a collaboration between the Max Delbrück Center for Molecular Medicine, the Weizmann Institute of Science, the Charité Berlin, the German Metrology Institute (PTB) and the Hasso Plattner Institute. The symposium is designed to provide an overview of state-of-the-art (pre)clinical UHF-MR and its synergies with data science, and to initiate local, regional, national and international collaboration and last but not least to provide plenty of opportunities to engage into fruitful exchange with peers and colleagues.

Message from the organizers

For the scientific program we are very much honored to present extraordinary speakers including MR technology leaders, leading data scientists, distinguished clinical experts and emerging scientists – all bridging disciplinary boundaries and stimulating the imaging community to throw further weight behind the solution of unsolved problems and unmet clinical needs. The scientific program comprises 4 sessions, all balancing technical developments, clinical applications and hot topics related to the synergies between imaging and data science. The scientific program is designed to lay extensive bridges between disciplines to enable the translation of multimodal AI technology into clinically-relevant imaging guided diagnostics, therapy monitoring and digital health applications.

We would like to draw your attention to the posters, all being made readily available for viewing and downloading. We wish to thank those of you who walked the extra mileage and submitted poster contributions. We really appreciate your efforts. Thanks to your valuable feedback we have also included several slots of 2 min enlightening poster power presentations into the program. This will give a large number of poster presenters the opportunity to be in the spotlight of the audience. Please support the poster presenters and do not miss to vote for the best poster.

Last but not least we wish to thank the MDC's event team for their tremendous support.

We very warm welcome you to Berlin and to ultrahigh field MR

Thoralf Niendorf
MDC & Charité, Berlin

Lucio Frydman
Weizmann Institute of Science, Rehovot, Israel

Jeanette Schulz-Menger
Charité, Berlin

Christoph Lippert
HPI, Potsdam

Michal Neeman
Weizmann Institute of Science, Rehovot, Israel

Sonia Waiczies
MDC, Berlin

Min-Chi Ku
MDC, Berlin

Sebastian Schmitter
PTB, Berlin

Grant Support

The organizers wish to acknowledge the generous support provided by the Deutsche Forschungsgemeinschaft (DFG), the German Research Foundation

About the DFG:

"The DFG is the self-governing organization for science and research in Germany. It serves all branches of science and the humanities. In organizational terms, the DFG is an association under private law. Its membership consists of German research universities, non-university research institutions, scientific associations and the Academies of Science and the Humanities.

The DFG supports projects from all scientific subject areas and especially promotes interdisciplinary cooperation between researchers. DFG funding enables cooperation between researchers from all branches of the science system as well as the formation of internationally conspicuous priorities at universities and non-university research institutions.

The foundation actively encourages international research cooperation: all of its programmes promote cooperation between scientists and academics in Germany and their colleagues abroad. It places special emphasis on collaboration in the scientific community in the European Research Area.

The DFG funds knowledge-oriented research and it welcomes and supports the cooperation of science with those who apply science in all areas of social life. This includes the interaction of scientific findings with industry and institutions like museums, academies of music, hospitals, and in public-private partnerships. Science and research are by definition international. Thus, the DFG's statutes include an obligation to foster contacts between scientists and researchers in Germany and abroad.

To advance internationalization, the DFG has opened its funding programmes for international collaboration between researchers – an absolute necessity for Germany in its role as a pioneering and simultaneously cosmopolitan centre of research and science."

Funded by

DFG Deutsche Forschungsgemeinschaft
German Research Foundation

For further details please visit: **www.dfg.de/en**

Table of Contents

MRI.TOOLS GmbH
innovations for medical imaging

RF Coils & Accesories for Animal and Human Imaging

We provide succesfully tested products as well as custom solutions that exactly meet your needs and specifications.

Our portfolio encompasses clinical and preclinical RF coils for field strength from 1.5 T to 11.5 T and for the nuclei of your choice.

With our coils, we provide a certificate issued by a notified body which confirms compliance with IEC 60601-1 and IEC 60601-2-33

Examples from our portfolio

32 channel modular transceiver array for cardiac/body imaging at 7.0 Tesla

8 channel transceiver array for carotid imaging at 3.0 Tesla

8 channel ^{1}H knee RF coil for pTX application at 7.0 Tesla

6 channel transceiver array for eye imaging at 3.0 Tesla and 7.0 Tesla

4 channel ^{23}Na and 4 channel ^{1}H RF coil for cardiac/liver imaging at 7.0 Tesla

^{19}F/^{1}H transceiver array for lung imaging at 3.0 Tesla and 7.0 Tesla

small monkey volume RF coil for brain imaging at 11.7 T

^{19}F/^{1}H volume RF coil for mouse imaging at 9.4 T

... and more

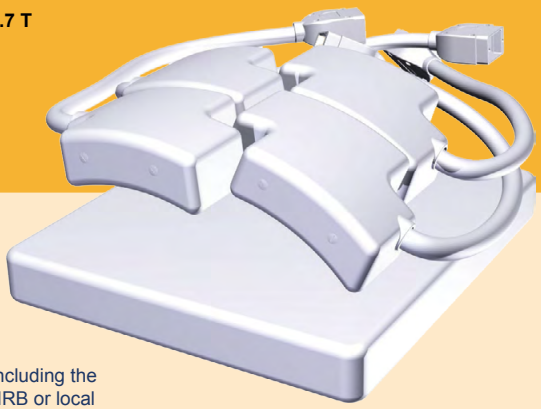

Device Testing and Certification

We offer dedicated consulting and testing services with the focus on in-house-built hardware including custom RF coils.

We prepare all documents and procedures including the certificate issued by a notified body for your IRB or local safety board.

Contact us:

www.mritools.de
info@mritools.de
+49 30 9489 2582

BRUKER

PRECLINICAL IMAGING

Ultra-High Field MRI

Cutting-edge sensitivity and resolution

Highest commercially available preclinical MRI instruments with field strengths of 11.7 Tesla, 15.2 Tesla, and 18 Tesla.

SCAN ME!

For more information please visit www.bruker.com

Organization

ORGANIZERS:

Thoralf Niendorf	Berlin, Germany (MDC & Charité)
Lucio Frydman	Rehovot, Israel (Weizmann Institute of Science)
Jeanette Schulz-Menger	Berlin, Germany (Charité & Helios Klinikum)
Michal Neeman	Rehovot, Israel (Weizmann Institute of Science)
Min-Chi Ku	Berlin, Germany (MDC)
Christoph Lippert	Potsdam, Germany (HPI)
Sebastian Schmitter	Berlin, Germany (PTB)
Sonia Waiczies	Berlin, Germany (MDC)

CONFERENCE OFFICE:

Lien-Georgina Dettmann, Matthias Runow & Timkehet Teffera
E-Mail: MRSymposium@mdc-berlin.de
Max Delbrück Center for Molecular Medicine in the Helmholtz Association
Robert-Rössle-Strasse 10
13125 Berlin
Phone: +49 30 9406 4824 / 3720 / 4255 / 2719

OFFICE PROF. NIENDORF:

Carolin Bechtloff: Carolin.Bechtloff@mdc-berlin.de
Max Delbrück Center for Molecular Medicine in the Helmholtz Association
Robert-Rössle-Straße 10
13125 Berlin
Phone: 0049 30 9406 3978

14TH ANNUAL SCIENTIFIC SYMPOSIUM ON ULTRAHIGH FIELD MAGNETIC RESONANCE

Friday, 8th September 2023

08:15	**WELCOME** chair: Thoralf Niendorf, Berlin, Germany Sonia Waiczies, Berlin, Germany
08:30	**KEYNOTE LECTURE** **Approaching the Summit: Insights from Magnetic Resonance Imaging at 10.5 T** Kamil Ugurbil, University of Minnesota, Minneapolis, USA

SCIENTIFIC SESSION I

GETTING TO THE MATTER OF THE HEART: CLINICAL NEEDS AND RESEARCH PROMISES OF CARDIOVASCULAR AND BODY UHF-MR

chair: Jutta Ellermann, Minneapolis, USA
Thoralf Niendorf, Berlin, Germany

08:50	**Getting to the Heart of the Matter: Advanced MRI of Ischemic Heart Disease** Hsin-Jung (Randy) Yang, Cedars Sinai, Los Angeles, USA
09:10	**Panta Rhei: Phase Contrast MRI at 7.0 T Improves Near-Wall Hemodynamic Parameters Quantification in Intracranial Aneurysms** Antoine Sache, Ecole Polytechnique Fédérale de Lausanne, Switzerland
09:30	**Mapping Out the Terrain: MR Fingerprinting Based Absolute Transmission Field Cartography in the Body with Low RF Power** Max Lutz, German Metrology Institute, Berlin, Germany
09:50	**What Lies Above Cardiac MRI at 7.0 T?** Bilguun Nurzed, Max Delbrück Center, Berlin, Germany

10:10	**POSTER POWER SESSION** (4 x 2 min) **Development and Evaluation of kT-point Pulses for Cardiac MRI at 7T** Sophia Nagelstraßer, Friedrich-Alexander-Universität Erlangen-Nürnberg (FAU), Germany **Characterizing Myocardial Perfusion and Early Signs of Myocardial Change in Hypertrophic Cardiomyopathy using Arterial Spin Labeling** Oumaima Laghzali, Max Delbrück Center, Berlin, Germany **Evaluating Cardiac Myosin Inhibitors for HCM: Insights from Advanced CMR Imaging and Histology in a Mouse Model** Siqin Liu, Max Delbrück Center, Berlin Germany **Advanced Cardiac MRI: Catching Heart Motion with Free-Running 3D Whole-Heart T2* mapping in Hypertrophic CardioMyopathy (HCM) model** Shahriar Shalikar, Max Delbrück Center, Berlin, Germany
10:20	**PANEL DISCUSSION: CARDIAC AND BODY MRI at UHF** chair: David Norris, Nijmegen, The Netherlands Sebastian Schmitter, Berlin, Germany
10:35	**COFFEE BREAK / RELAXATION WITH LIVE MUSIC**

SCIENTIFIC SESSION II

GETTING TO THE MATTER OF THE BRAIN: CLINCIAL NEEDS AND RESEARCH PROMISES FOR NEUROVASCULAR UHF-MR AND RELATED FIELDS

chair: Santosh Kumar Maurya, Rehovot, Israel
Min-Chi Ku, Berlin, Germany

10:55	**Next Generation Tools for Data Science Innovation in Imaging** Amina Chebira, Flywheel Inc, Lausanne, Switzerland
11:15	**Assessment of Multiple Sclerosis: Lessons Learnt from UHF-MRI** Russell Ouellette, Karolinska Institute, Stockholm, Sweden
11:35	**Probing Human Brain Glucose Metabolism: Direct (2H) and Indirect (1H) Detection of Deuterium Labeled Substrates at 7.0 T** Fabian Niess, Medical University of Vienna, Austria

Program September 8, 2023

11:55	**Rich Opportunities for Discovery: The Dutch National 14.0 T MRI Initiative in Medical Science** David Norris, Donders Institute for Brain Cognition and Behaviour, Nijmegen, The Netherlands
12:15	**POSTER POWER SESSION** (6 x 2 min) **The Brain Age Gap Estimation (BrainAGE) Predicts Brain Reserve Estimated Using a Residual Approach in Alzheimer's Continuum** Ersin Ersoezlue for the Alzheimer's Disease Neuroimaging Initiative (ADNI) study Department of Psychiatry and Psychotherapy, University Hospital, LMU Munich, Germany **Rapid PD, T2, and T2* Mapping in Multiple Sclerosis Using 2in1-RA-RE-EPI and Model-Based Reconstruction** Jose Raul Velasquez Vides, Max Delbrück Center, Berlin, Germany **Role of Map Based High Order Shimming for Single Voxel Spectroscopy (SVS) at 7T** Hoby Hetherington, Department of Radiology University of Missouri, USA **A Triple CycleGAN Model Ensemble for Motion Correction in 7T MR Brain Imaging** Gulfam Ahmed Saju, University of Massachusetts Dartmouth, USA **Study of Radiofrequency-Induced Heating Inside the Human Head with Dental Implants at 7 T** Xuegang Xin, South China University of Technology, Guangzhou, Guangdong, China **Advancing 7T BOLD fMRI Spatial Accuracy and Sensitivity: Unveiling Individual Brain Neurosignatures** Igor F. Tellez Ceja, Max Delbrück Center, Berlin, Germany
12:25	**PANEL DISCUSSION: BRAIN MRI AT UHF** chair: Sonia Waiczies, Berlin, Germany Alexandre Vignaud, Saclay, France
12:40	**LUNCH BREAK / BREAKFAST BREAK**

SCIENTIFIC SESSION III

TRANSLATIONAL RESEARCH: FROM BLUE SKY EXPLORATIONS EN ROUTE TO CLINICAL APPLICATIONS

chair: Kamil Ugurbil, Minneapolis, USA
Nandita Saha, Berlin, Germany

13:25	**Imaging Mini Brains: Artificial Intelligence for High Field MRI of Cerebral Organoids** Luca Deininger, Karlsruhe Institute of Technology, Eggenstein-Leopoldshafen, Germany
13:45	**The Kidney is a Remarkable Organ: In Vivo Monitoring of the Renal Tubule Volume Fraction Using Parametric MRI** Ehsan Tasbihi, Max Delbrück Center, Berlin, Germany
14:05	**A Toolbox to Probe Oxygenation and Inflammation in Disease Models with 19F MRI** Sebastian Temme, University of Düsseldorf, Germany
14:25	**Turning a Diagnostic Instrument into a Therapeutic Device: Helmet RF Applicators for Thermal MR at 7.0 T** Faezeh Rahimi, Max Delbrück Center, Berlin, Germany
14:45	**Sea to Summit: Progress in Preclinical MR at Ultrahigh and Extreme Magnetic Fields** Tim Wokrina, Bruker Biospin MRI GmbH, Ettlingen, Germany

Program September 8, 2023

15:05	**POSTER POWER SESSION** (4 x 2 min) **Monitoring of Timed Degradation of Biodegradable Metal Implants: How MRI Can Contribute** Martin Meier, ZTL Imaging-Center, Hannover Medical School, Germany **Dynamic MRI and Deep Learning: Tracking Acute Kidney Size Changes in Rats** Tobias Klein, Max Delbrück Center, Berlin, Germany **Improving B1+ Homogeneity in Brain imaging at 7 T with A Flexible Metasurface-Based Pad** Vladislav Koloskov, ITMO University, St. Petersburg, Russia **Evaluation of Dipole Antenna RF Applicators for ThermalMR Theranostics** Nandita Saha, Max Delbrück Center, Berlin, Germany
15:15	**PANEL DISCUSSION: TRANSLATIONAL MRI AT UHF** chair: Jason Millward, Berlin, Germany Alexander Raaijmakers, Eindhoven and Utrecht, The Netherlands
15:30	**COFFEE BREAK / RELAXATION WITH LIVE MUSIC**

Program September 8, 2023

SCIENTIFIC SESSION IV

LOOKING AT THE HORIZON

chair: Franz Schmitt, Quetzin, Germany
Bernd Ittermann, Berlin, Germany

15:55	**From Acoustics to MRI: Manipulation of Wave Propagation to Boost Transmission Efficiency and Sensitivity with Metamaterials** Santosh Kumar Maurya, Weizmann Institute of Science, Rehovot, Israel
16:15	**Scaling the Mountains: Progress and Challenges of Commissioning the Iseult CEA 11.7 T Whole-Body MRI Instrument** Alexandre Vignaud, Neurospin CEA, Saclay, France
16:35	**Let's Climb The Mountains: RF Array Concepts for Brain MRI at 14.0 T** Alexander Raaijmakers, Technical University Eindhoven and Utrecht Medical Center, The Netherlands
16:55	**About Mountaineers and Explorers: Germany's Journey Toward 14.0 T Human Magnetic Resonance** Thoralf Niendorf, Max Delbrück Center, Berlin Germany
17:15	**Mountaineering Tools and Their Uses: Progress in UHF-MR Technology and Applications** Robin Heidemann, Siemens Healthineers, Erlangen, Germany
17:35	**PANEL DISCUSSION: FUTURE OF UHF MRI** chair: Kamil Ugurbil, Minneapolis, USA Bernd Ittermann, Berlin, Germany
18:00	Get Together

13490 0323

MAGNETOM Terra.X

Make the difference.

siemens-healthineers.com/terrax

MAGNETOM Terra.X* introduces the next generation 7T MRI that will enable you to make the difference. With its groundbreaking Ultra IQ Technology, it will deliver unprecedented image clarity that allows you to confidently assess subtle pathological details. In combination with our AI-powered Deep Resolve, MAGNETOM Terra.X ultimately will take clinical routine to a new level. MAGNETOM Terra.X makes the difference for clinicians and scientists.

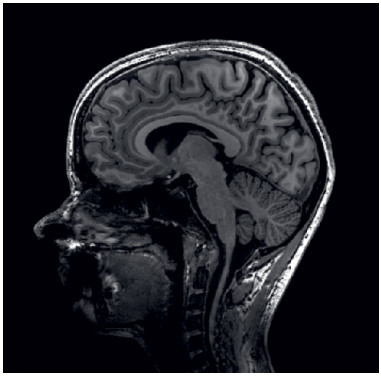

StudyID: 4aaaa0264 / 8Tx32Rx head coil

** MAGNETOM Terra.X is still under development and not commercially available yet. Its future availability cannot be ensured.*

SIEMENS Healthineers

Poster Abstracts

(In alphabetical order)

P1

The Brain Age Gap Estimation (BrainAGE) Predicts Brain Reserve Estimated Using a Residual Approach in Alzheimer's Continuum

Ersin Ersoezlue[1,2] *and Boris-Stephan Rauchmann*[1,3,4,5] *for the Alzheimer's Disease Neuroimaging Initiative (ADNI) study*

[1] *Department of Psychiatry and Psychotherapy, University Hospital, LMU Munich, Munich, Germany*

[2] *Department of Geriatric Psychiatry and Developmental Disorders, kbo-Isar-Amper-Klinikum Munich East, Munich, Germany*

[3] *Department of Neuroradiology, University Hospital, LMU Munich, Munich, Germany*

[4] *German Center for Neurodegenerative Diseases (DZNE), Munich, Germany*

[5.] *Sheffield Institute for Translational Neurology (SITraN), University of Sheffield, Sheffield, UK*

Background

Resilience refers to multiple reserve-related processes, e.g., cognitive reserve (CR) and brain reserve (BR) (Stern et al. 2020; Ossenkoppele et al. 2020), while facing alterations in the brain, i.e., aging or neurodegenerative disease such as Alzheimer's disease (AD). The Brain Age Gap Estimation (BrainAGE) algorithm is developed to estimate morphological brain age, which was suggested to be affected by various neurological and psychiatric diseases, including preclinical and clinical AD (Gaser et al. 2013). We aim to test possible associations between BrainAGE and brain reserve and how AD-specific multimodal imaging biomarkers modify this association.

Methods and Participants

The study cohort resulted in N=195 (Amyloid beta) Aβ negative and cognitively normal healthy controls (HC, 71 years, 119 female) and N=264 Aβ positive participants (AD, 74 years, 142 female; N=175 A+T- and N=89 A+T+) as Alzheimer's continuum. The participants underwent structural T1-MPRAGE MRI imaging, Aβ PET and tau PET. BR was calculated as the residualized global cortical volume by tau composite score, defined in AD-specific regions. CR was defined as a residualized global cognitive composite score by demographics (age and sex), study sites and tau PET and Aβ PET as predictors. BrainAGE was obtained as the gap between the brain age estimated from MR images and the actual chronological age (Franke et al. 2010). We then calculated inverse BrainAGE (InvBrainAGE) to estimate resilience using positive values. The statistical models were conducted in the entire cohort and adjusted for demographics, APOE4-status, Amyloid/Tau(AT)-Status, and study sites, while the linear mixed models were adjusted additionally for clinical diagnosis. Longitudinal observations of the Mini-Mental State Examination (MMSE) and Clinical Dementia Ratio-Sum of Boxes (CDR-SoB) up to two years were tested in separate models for BR and InvBrainAGE.

Results

InvBrainAGE was predicted by higher BR (b=0.38, p<0.001, R^2adjusted=0.19), but not with CR (b=0.09, p=0.08, R^2adjusted=0.06) (**Figure 1**). Both BR and InvBrainAGE were related to slower cognitive decline over time in interaction with CR (MMSE: BR*CR*Time p<0.001 and InvBrainAGE*CR*Time p=0.03; CDR-SoB: BR*CR*Time p=0.09 and InvBrainAGE*CR*Time p=0.03) (**Figure 2**).

Conclusions

InvBrainAGE was moderately associated with BR and could estimate the longitudinal effects of brain reserve. Our results suggest an operational value of InvBrainAGE as a brain reserve proxy, having a significant advantage, being a unimodal approach in contrast to the residual approach to estimate BR.

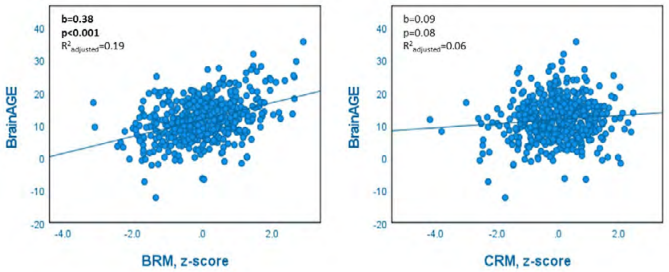

Figure 1. The scatter plots of associations between (Inverse)BrainAGE and residual markers of brain reserve (BRM) and cognitive reserve (CRM).

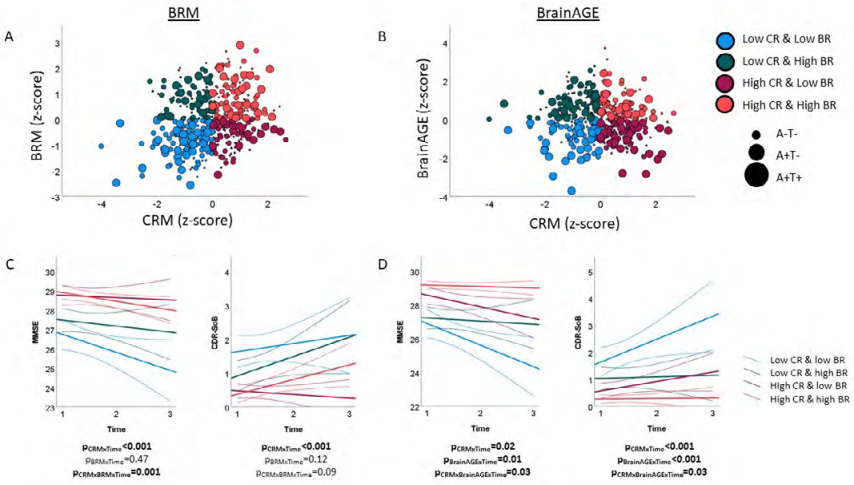

Figure 2. A-B: The scatter plots of (Inverse)BrainAGE and residual markers of brain and cognitive reserve (BRM, CRM). C-D: Longitudinal trajectories of Mini-Mental State Examination (MMSE) and Clinical Dementia Ratio-Sum of Boxes (CDR-SoB) among groups presented using a median split for visual purposes, while analyses were conducted using continuous variables.

P2

Role of Map Based High Order Shimming for Single Voxel Spectroscopy (SVS) at 7T

Hoby Hetherington[1,2], *Melissa Terpstra*[1], *Chan Moon*[3], *Junghwan Kim*[1], *Jullie Pan*[1]

[1] *Department of Radiology University of Missouri*

[2] *Resonance Research Inc.*

[3] *Department of Radiology University of Pittsburgh*

Although achieving sufficient B0 homogeneity is a requirement for in vivo brain spectroscopy, the extent to which inhomogeneities higher than 2nd order contribute to the achievable homogeneity for single voxel acquisitions and the ability of higher order shims to correct them has been questioned. To assess these questions, we acquired SVS from two loci of clinical interest, the rostral prefrontal cortex (rPFC) and hippocampus (Hc) using voxels of 8 and 9cc respectively. The rPFC is characterized by large susceptibility gradients over a few millimeter distances, which can often result in insufficient homogeneity after shimming resulting in a trial-and-error approach to voxel positioning.

To address this issue in the rPFC, we developed an automated routine, SUsceptibility-Managed-Optimization, (SUMO) to predict the achievable B0 homogeneity using a single initial whole brain B0 map. For the 8cc voxel and target location, the SUMO search over a 27x27x21mm region (<5sec) successfully identified a voxel with a predicted standard deviation of residual inhomogeneity (σ_(B0)) below the user-chosen threshold of 5Hz after 1st-4th order shimming. In the SUMO-identified voxel we compared two shim strategies: our map-based shimming method (BOLERO), and a projection-based method, FAST(EST)MAP. We also compared the shimming using the vendor's 1st&2nd order shims with that achievable adding in 3rd-4th order shims from a commercially available shim insert. The 7T SVS acquisition used STEAM, TR/TM/TE of 6s/20ms/8ms, a tissue water acquisition for concentration reference and LCModel for spectral analysis.

In the rPFC (n=7 subjects), the use of BOLERO reduced the inhomogeneity seen with FAST(EST)MAP from σB0= 9.8±4.5Hz to σB0= 6.5±2.0Hz when using the same shim hardware. The shim insert (3rd and 4th order shims) further reduced σB0 to 4.0±0.8Hz. In the Hc (n=7 subjects), FAST(EST)MAP, Bolero with 1st-2nd order shims and Bolero with 1st-4th order shims achieved σB0 values of 8.6±1.9, 5.6±1.0 and 4.6±0.9 Hz respectively. σB0 was significantly correlated with the CRLBs and concentrations of inositol, glutamate, and glutamine in the rPFC. In addition to decreasing σB0, Bolero with 1st-4th order shims also improved the lineshape returning a more gaussian lineshape, which was correlated with reduced variance in metabolite con-

tent. Overall, the use of the high order and map based B0 shim methods improved the accuracy and consistency of spectroscopic data.

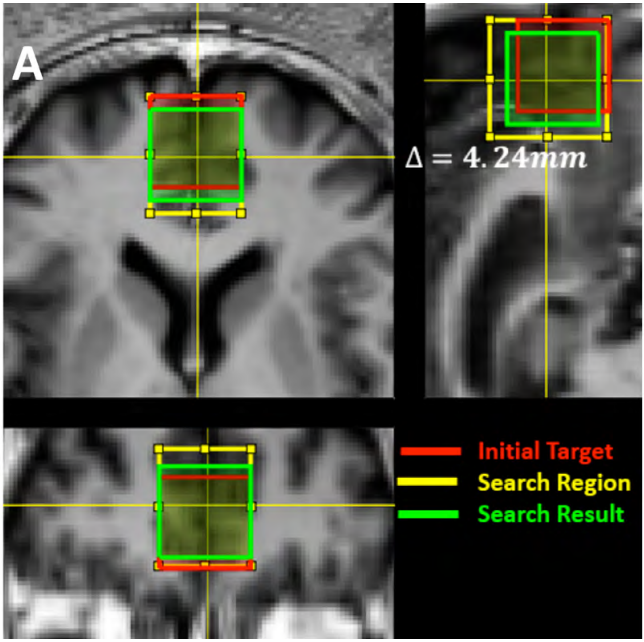

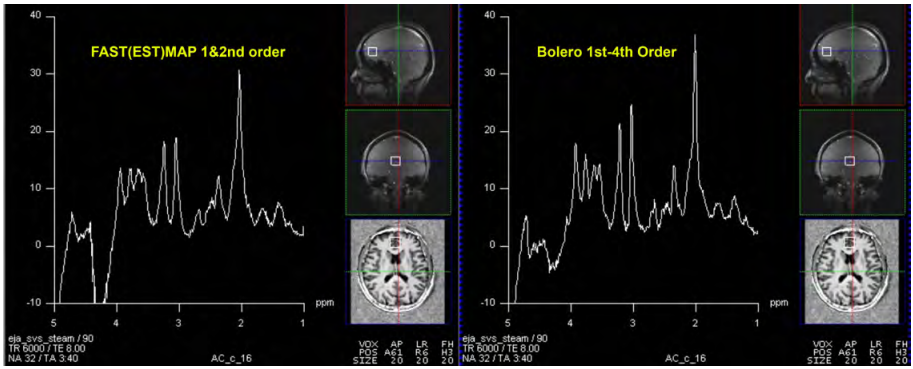

Picture description
Schematic of SUMO process. The initial target location is shown in red. The search region is displayed in yellow. The closest voxel within the search region to the target voxel achieving a σB0<5Hz is identified in green. It is 4.24mm away from the target region. On average, the σB0 decreased from 9.2+/- 3.6Hz at the initial target location to 4.0+/-0.8Hz at the selected region corresponding to a move of 4.2+/-2.1mm

Spectra acquired from the rPFC using FAST(EST)MAP and Bolero 1st-4th order shimming.

P3

Dynamic MRI and Deep Learning: Tracking Acute Kidney Size Changes in Rats

Tobias Klein[1,2], *Thomas Gladytz*[1], *Jason M. Millward*[1], *Kathleen Cantow*[3], *Luis Hummel*[3], *Erdmann Seeliger*[3], *Sonia Waiczies*[1], *Christoph Lippert*[2, 4], *Thoralf Niendorf*[1,5]

[1]*Berlin Ultrahigh Field Facility (B.U.F.F.), Max Delbrück Center for Molecular Medicine in the Helmholtz Association, Berlin, Germany*

[2]*Digital Health Machine Learning Research Group, Hasso Plattner Institute for Digital Engineering, University of Potsdam, Germany*

[3]*Institute of Translational Physiology, Charité – Universitätsmedizin, Berlin, Germany*

[4]*Hasso Plattner Institute for Digital Health, Icahn School of Medicine at Mount Sinai, New York City, USA*

[5]*Experimental and Clinical Research Center, a joint cooperation between the Charité Medical Faculty and the Max Delbrück Center for Molecular Medicine, Berlin, Germany*

Introduction

Kidney diseases pose a significant health concern. An increasing body of literature emphasizes the potential of non-invasive imaging in assessing renal size for the diagnosis, treatment, and prognosis of renal disease1-6. Manual segmentation limitations prompt automated alternatives like machine learning (ML)7-9. However, the role of ML in dynamic MRI-based kidney size monitoring remains unexplored. Here we investigated the applicability of a deep dilated U-Net (DDU-Net) for MR-based kidney size (KS) assessment in rats with the goal to capture and quantify acute changes in kidney size (ΔKS) during clinically relevant interventions.

Methods

We acquired T2-weighted 2D kidney images from 52 rats10. Manual segmentation established the ground truth from baseline T2-maps of 43 rats for DDU-Net training and validation. For testing, 29 rats underwent interventions: aortic occlusion, venous occlusion, simultaneous occlusion, furosemide administration, hypoxemia, and X-ray contrast medium injection10-12.

Compared to the original U-Net, DDU-Net extended receptive field through extra layers and skip-connections8,9. DDU-Net's performance was evaluated against an analytical bean shape model (ABSM) and the nnU-Net using simulated data (400 scenarios)10,13. Finally, DDU-Net was applied on the longitudinal in vivo intervention data to detect and quantify relative changes in kidney size.

Results

DDU-Net and ground truth yielded mean KS of 211 ± 1 mm². DDU-Net showed R^2 0.92 (Fig. 1), MAPE 1.1%, Dice score 0.98, and median intra-subject variability 0.3% versus the ground truth. The corresponding results obtained for the nnU-Net were 0.91,

1.2%, and 0.3%,. Simulated data demonstrated DDU-Net's superiority in MAPEs (73% vs. ABSM, p < 10-20; 51% vs. nnU-Net, p > 0.05). For SNR > 2.5 and CRF > 0.25, DDU-Net excelled (89%, p < 10-41), as did nnU-Net (57%, p < 10-2), with median MAPE of 1.0% (Fig. 2).

DDU-Net detected ΔKS of -8 ± 1% (aortic occlusion), 5 ± 1% (venous occlusion), -3 ± 1% (simultaneous occlusion) (Fig. 3), 2 ± 1% (furosemide), -2 ± 1% (hypoxemia), and up to 11 ± 1% (X-ray CM injection) (Fig. 4).

Discussion

DDU-Net is very well suited for rapid segmentation of rat kidney. It facilitates quantification of relative changes in kidney size which are in the range of a single-digit percentage and larger. The proposed DDU-Net approach enables real-time renal size assessment, is scalable to 3D. A modified version of our DDU-Net implementation would support kidney segmentation from MR images obtained from population studies and would help to enhance our understanding of renal disease determinants.

References

1. Hoste EAJ, Kellum JA, Selby NM, et al. Global epidemiology and outcomes of acute kidney injury. Nat Rev Nephrol. Oct 2018;14(10):607-625. doi:10.1038/s41581-018-0052-0
2. Levin A, Tonelli M, Bonventre J, et al. Global kidney health 2017 and beyond: a roadmap for closing gaps in care, research, and policy. The Lancet. 2017;390(10105):1888-1917. doi:10.1016/s0140-6736(17)30788-2
3. Luyckx VA, Tonelli M, Stanifer JW. The global burden of kidney disease and the sustainable development goals. Bull World Health Organ. Jun 1 2018;96(6):414-422D. doi:10.2471/BLT.17.206441
4. Global, regional, and national burden of chronic kidney disease, 1990-2017: a systematic analysis for the Global Burden of Disease Study 2017. Research Support, Non-U.S. Gov't. Lancet. Feb 29 2020;395(10225):709-733. doi:10.1016/S0140-6736(20)30045-3
5. Periquito JS, Gladytz T, Millward JM, et al. Continuous diffusion spectrum computation for diffusion-weighted magnetic resonance imaging of the kidney tubule system. Quant Imaging Med Surg. Jul 2021;11(7):3098-3119. doi:10.21037/qims-20-1360
6. van Duijl TT, Ruhaak LR, de Fijter JW, Cobbaert CM. Kidney Injury Biomarkers in an Academic Hospital Setting: Where Are We Now? Clin Biochem Rev. May 2019;40(2):79-97. doi:10.33176/AACB-18-00017
7. Sharma K, Rupprecht C, Caroli A, et al. Automatic Segmentation of Kidneys using Deep Learning for Total Kidney Volume Quantification in Autosomal Dominant Polycystic Kidney Disease. Sci Rep. May 17 2017;7(1):2049. doi:10.1038/s41598-017-01779-0
8. Ronneberger O, Fischer P, Brox T. U-Net: Convolutional Networks for Biomedical Image Segmentation. presented at: MICCAI; 2015;
9. Wang S, Singh VK, Cheah E, et al. Stacked dilated convolutions and asymmetric architecture for U-Net-based medical image segmentation. Comput Biol Med. Sep 2022;148:105891. doi:10.1016/j.compbiomed.2022.105891
10. Gladytz T, Millward JM, Cantow K, et al. Reliable kidney size determination by magnetic resonance imaging in pathophysiological settings. Acta Physiol (Oxf). Oct 2021;233(2):e13701. doi:10.1111/apha.13701
11. Cantow K, Evans RG, Grosenick D, et al. Quantitative Assessment of Renal Perfusion and Oxygenation by Invasive Probes: Basic Concepts. Methods Mol Biol. 2021;2216:89-107. doi:10.1007/978-1-0716-0978-1_6

12. Cantow K, Gladytz T, Millward JM, Waiczies S, Niendorf T, Seeliger E. Monitoring kidney size to interpret MRI-based assessment of renal oxygenation in acute pathophysiological scenarios. Acta Physiol (Oxf). Aug 22 2022:e13868. doi:10.1111/apha.13868

13. Isensee F, Jaeger PF, Kohl SAA, Petersen J, Maier-Hein KH. nnU-Net: a self-configuring method for deep learning-based biomedical image segmentation. Nat Methods. Feb 2021;18(2):203-211. doi:10.1038/s41592-020-01008-z

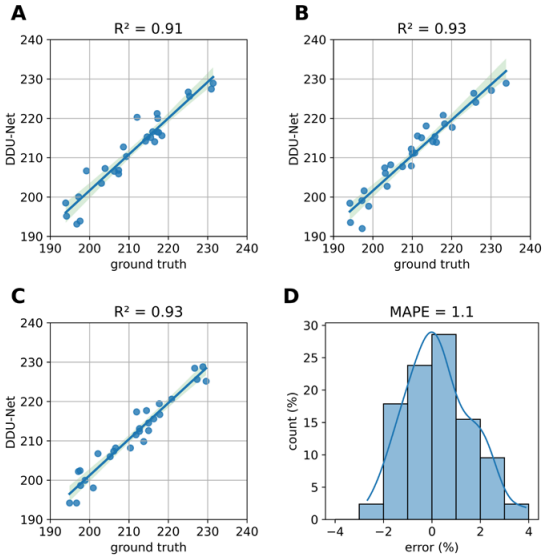

Figure 1

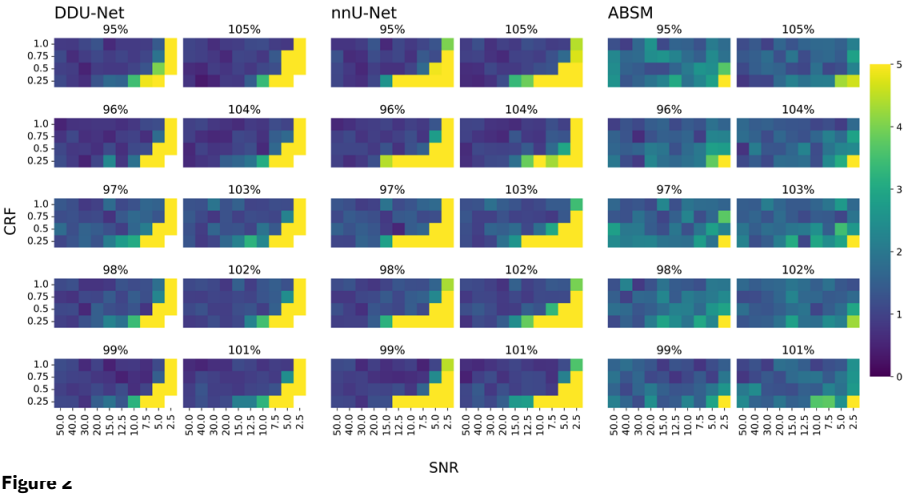

Figure 2

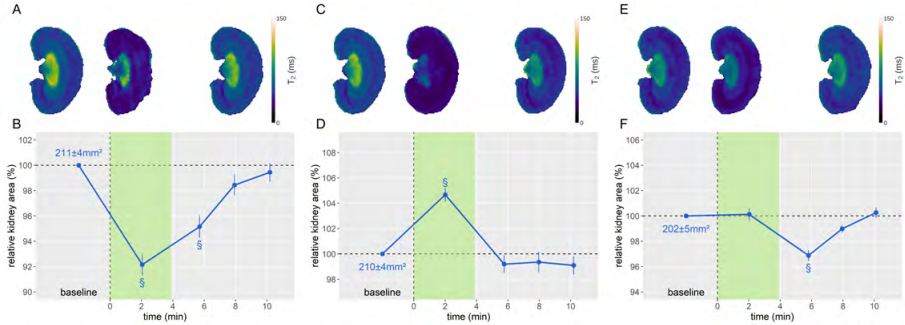

Figure 3

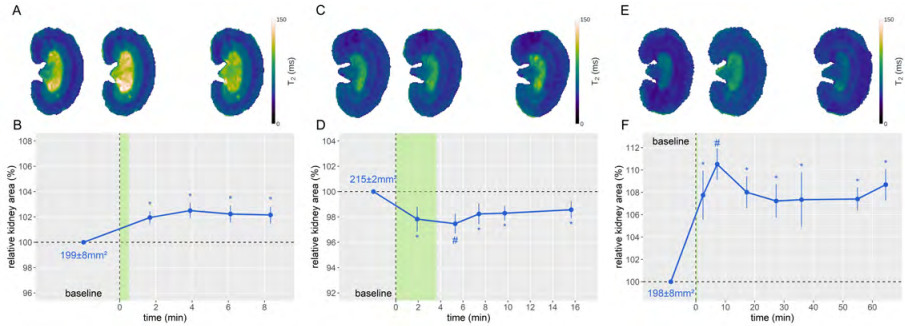

Figure 4

Picture description

Fig. 1. A-C: Linear regression plots (blue) including the 95 % confidence interval (green) and the identity (gray) for the ground truth KS and predicted KS by the DDU-Net for each baseline map. D) Distribution of the residuals between ground truth and predicted KS for all three baseline maps yielding an average MAPE of 1.1 %.

Fig. 2. Assessment of DDU-Net, nnU-Net and ABSM approach using simulated data and the metric MAPEs. The figure summarizes MAPEs achieved by DDU-Net, nnU-Net, and the ABSM for every combination of SNR (from 2.5 to 50), CRF (from 0.25 to 1.0), and relative KS (from 95 % to 105 %). White spots indicate a failure to segment the kidney for simulated data using very low SNRs, which are not realistic for real world MRI examinations.

Fig. 3. T2 maps acquired before, during, and after occlusion of the A) suprarenal aorta, C) renal vein, and E) both vessels. B/D/F: Relative KS over time for the respective intervention. The intervention period is highlighted in green. (Dunn's post hoc test. With $\alpha = 0.05$, a $p < \alpha / 2 = 0.025$ was considered to be statistically relevant. §: $p < 0.001$, #: $p < 0.01$)

Fig. 4. T2 maps acquired before, upon, and after A) administration of furosemide, C) hypoxia, and E) administration of an X-ray CM. B/D/F: Relative KS over time for the respective intervention. The intervention period is highlighted in green. (Dunn's post hoc test. With $\alpha = 0.05$, a $p < \alpha / 2 = 0.025$ was considered to be statistically relevant. §: $p < 0.001$, #: $p < 0.01$, *: $p < 0.025$)

P4

Improving B1+ homogeneity in brain imaging at 7 T with flexible metasurface-based pad

Vladislav Koloskov[1], *Wyger M. Brink*[2,3], *Andrew G. Webb*[3], *and Alena Shchelokova*[1]

[1] *School of Physics and Engineering, Faculty of Physics, ITMO University, St. Petersburg, Russia*

[2] *Magnetic Detection & Imaging Group, TechMed Centre, University of Twente, Enschede, The Netherlands*

[3] *C.J. Gorter MRI Center, Department of Radiology, Leiden University Medical Center, Leiden, The Netherlands*

Ultra-high field MRI allows one to perform better MR imaging and obtain a higher spatial resolution than clinical MR systems. However, dielectric artifacts and tissue heating can be faced. Previously shown artificial structures used for passive shimming have drawbacks like bulkiness, deterioration of properties in time, and anisotropy. Here we demonstrate numerically and experimentally the use of light and flexible metasurface to tailor B1+ distribution to achieve high homogeneity in the brain at 7T MRI.

The proposed metasurface (MS) consists of a set of metal crosses connected with capacitors (Fig. 1). Optimization based on variation of capacitors' values with fixed geometrical properties of the unit cell was performed with the following goal functions: the proposed structure should be a non-resonant on the working frequency of 298 MHz and tailor B1+ field to its max homogeneity in the ROI. Numerical electromagnetic simulations were done using CST MW Studio 2021. A head birdcage coil (BC) loaded with a male voxel model was used for all setups. To evaluate the effect of the MSs, we investigated B1+ maps and SAR maps averaged over 10 grams of tissues (SARav.10g). Both were normalized to 1W of the total accepted power. Experimental studies with a male volunteer were performed on a Philips 7T Achieva MRI system with a quadrature transmit head coil and a 32-ch receive phased array.

The optimization resulted in two setups: (1) two MSs (4.8 pF and 7 pF) located near the left and right temporal lobe, and (2) one MS (4.8 pF) placed near the occipital lobe. Figure 2 (A-C) shows the |B1+|RMS maps for a reference case, a setup with two MSs and one MS. The mean B1+ value throughout the whole brain was increased by 3% for both cases. Homogeneity was improved by 1% in ROI1, 5% in ROI2 for the first setup, and 10% in ROI3 for the second setup. Hot spots with max SAR values stayed unchanged in values and positions. Fig. 3 (A-F) shows tailored B1+ distribution in the ROIs with the same patterns as in the numerical study. One can observe improved quality of T1-weighted images (Fig. 3 (G-L)) in the case of MSs placement. ROIs have more detailed brain structures, better tissue contrast, and extended region of visualization in the occipital lobe.

It was numerically and experimentally shown that the light and flexible metasurfaces can effectively eliminate magnetic field minima in temporal lobes caused by a standing wave at 7T MRI.

P5

Characterizing Myocardial Perfusion and Early Signs of Myocardial Change in Hypertrophic Cardiomyopathy using Arterial Spin Labeling

Oumaima Laghzali[1,2], *Shahriar Shalikar*[1], *Siqin Liu*[1,2], *Frank Kober*[3], *Sonia Waiczies*[1], *Thoralf Niendorf*[1,2,4], *Min-Chi Ku*[1,2]

[1]*Berlin Ultrahigh Field Facility (B.U.F.F.), Max Delbrueck Center for Molecular Medicine in the Helmholtz Association, Berlin, Germany*

[2]*DZHK (German Centre for Cardiovascular Research), partner site Berlin, Germany*

[3]*Centre de Resonance Magnetique Biologique et Medicale (CRMBM), Aix-Marseille University, CNRS, Marseille, France.*

[4]*Experimental and Clinical Research Center, Charite Medical Faculty and the Max Delbrueck Center for Molecular Medicine in the Helmholtz Association, Berlin, Germany*

Given the prevalence of cardiomyopathies in young patients, early dysfunction detection is vital. Hypertrophic cardiomyopathy (HCM), a genetic disease with links to cellular remodeling, microvasculature damage, and myocardial fibrosis [1]. Perfusion deficits precede clinical symptoms like left ventricular hypertrophy (LVH) [2]. [2]. Our aim is to use cardiac magnetic resonance imaging (CMR) as a non-invasive tool to detect early signs of HCM and gain a better understanding of the early mechanisms of the disease. In this study, we use arterial spin labeling (ASL) as a reliable sensitive technique [3] to quantify resting myocardial tissue perfusion in a HCM mouse model that mimics human disease and detects any deficit occurring at an early stage.

We quantified the myocardial blood flow (MBF) of 10 weeks old (n=9) wildtype controls (WT), heterozygous (HET) and homozygous Mybpc3-KI (KI) mice inC57BL/6J background at 9.4 T (Biospec 94/20, Bruker, Germany). Cine ASL-CMR was acquired using the following parameters: TR/TE = 6.7/1.5 ms, FA = 6°, FOV = 25 × 25mm2, matrix size = 128 × 128, slice thickness = 1 mm, 25 averaged cine blocks for both tag and control images.

All mice underwent The functional analysis based on the AHA 17 segment model and obtained using the freely available software Segment v4. 0 R (Medviso, segment. heiberg.se). The perfusion maps were generated using in-house developed analysis tools built in the Interactive Data Language (IDL). Myocardial perfusion values were then assessed by delineating various regions of interest, based on the LV segmentation model, within the mid-ventricle of the LV myocardium.

KI mice displayed pronounced left ventricular hypertrophy (LVH) and reduced ejection fraction (LVEF) compared to WT and HET ($p<0.05$). Resting global myocardial blood flow (MBF) was lower in KI and HET compared to WT (End diastole: MBFKI = 6.38 ml/g/min, MBFHET = 6.86 ml/g/min, MBFWT = 8.90 ml/g/min, $p<0.001$) (End

systole: MBFKI = 6.09 ml/g/min, MBFHET = 6.01 ml/g/min, MBFWT = 8.34 ml/g/min, p<0.001).

This study demonstrates cine-ASL's sensitivity in detecting perfusion deficiency in a humanized HCM mouse model, aligning with previous research [3]. Heterozygous HCM mice show decreased MBF, yet preserved ejection fraction, indicating early microvascular dysfunction. Combining quantitative CMR techniques with histological findings holds promise for understanding disease mechanisms and averting critical cardiac events.

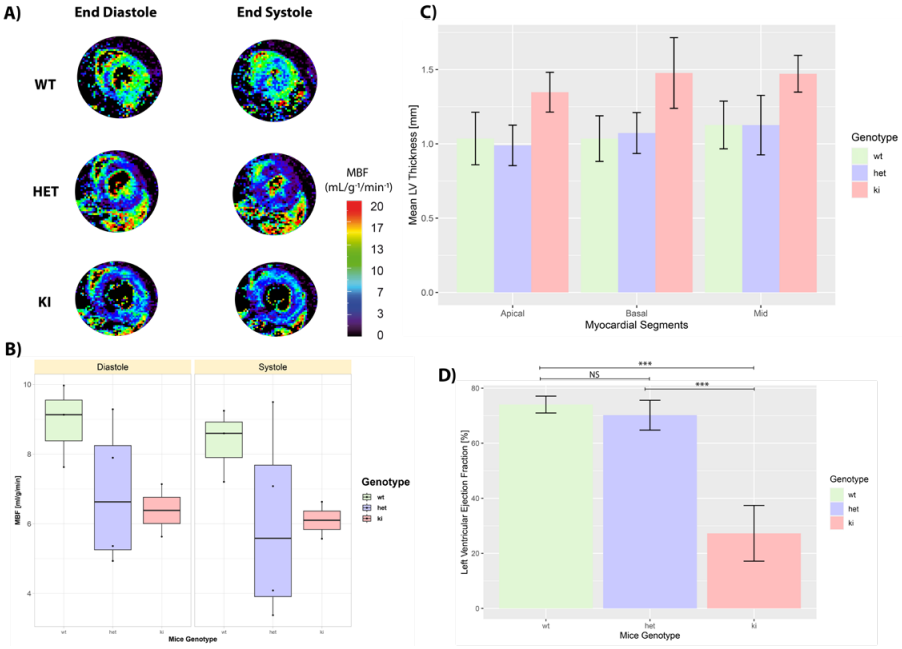

Picture description

Myocardial perfusion maps are sensitive to early myocardial change in heterozygous mybpc3 mice. A) Representative perfusion maps showing mid ventricular SAX view in both end systolic and end diastolic phase, the WT control mice show higher value maps compared to other genotypes. B) Results of mean MBF from the full myocardium show significant difference between HET and KI mice compared to control mice. C) Manual segmentation of the myocardium and analysis according to 17 AHA segments revealed LVH in KI but no significant differences between HET and WT mice. D) Functional analysis shows a preserved left ventricular ejection fraction of HET mice compared to KI mice. WT: wildtype, HET: heterozygous, KI: knocked in, MBF: myocardial blood flow, LVH: left ventricular hypertrophy.

P6

Evaluating Cardiac Myosin Inhibitors for HCM: Insights from Advanced CMR Imaging and Histology in a Mouse Model

Siqin Liu [1,2], *Oumaima Laghzal* [1,2], *Thoralf Niendorf* [1,2,3], *Sonia Waiczies* [1], *Min-Chi Ku* [1,2]

[1]*Berlin Ultrahigh Field Facility (B.U.F.F.), Max Delbrueck Center for Molecular Medicine in the Helmholtz Association, Berlin, Germany*

[2]*DZHK (German Centre for Cardiovascular Research), partner site Berlin, Germany*

[3]*Experimental and Clinical Research Center, Charite Medical Faculty and the Max Delbrueck Center for Molecular Medicine in the Helmholtz Association, Berlin, Germany*

Hypertrophic cardiomyopathy (HCM) is a heart condition characterized by the thickening of the heart muscle, which impairs the heart's ability to pump blood effectively. Current therapies for HCM, such as blockers and calcium channel blockers, have shown limited efficacy in managing the symptoms of the disease. Some medications used in the treatment of heart failures, such as angiotensin-converting enzyme inhibitors and angiotensin receptor blockers, have shown potential benefits in mitigating myocardial remodeling.

As a potential therapeutic target in HCM, cardiac myosin, a major component of muscle tissue, has garnered attention. Mavacamten, a first-in-class cardiac myosin inhibitor, directly modulates cardiac -myosin, leading to the reversible inhibition of actin-myosin cross-bridging. Promising results have been observed in clinical trials with the use of echocardiograms and blood biomarkers, indicating the potential effectiveness of myosin inhibitors in HCM to reduce of myocardial hypertrophy and improve cardiac function. However, to gain a comprehensive understanding of the treatment's impact, further evidence from the level of tissue remodeling is essential.

The primary objective of this study is to utilize quantitative cardiac magnetic resonance imaging (CMR) and histological assessments to confirm the effectiveness of the cardiac myosin inhibitor in HCM based on the level of myocardial remodeling. Given the challenges of obtaining histological and imaging data from human patients with HCM, we have employed an HCM mouse model in our study. This mouse model carries a point mutation in the cardiac myosin-binding protein C (cMYBP-C), which is known to be one of the most frequent mutations observed in HCM populations. Utilizing this mouse model allows us to closely mimic HCM pathophysiology in a controlled environment, providing valuable data for the study.

Our preliminary CMR data has already shown noticeable differences between HCM mice and wildtype mice at the baseline before drug treatment (Fig. 1). We will conduct further in-depth investigations to comprehensively analyze the effects of the cardiac myosin inhibitor (Fig. 2). The next step in our research is to administer the drug to the HCM mice and assess its efficacy in mitigating the heart muscle thickening

and other signs of myocardial remodeling. Through our research, we hope to shed light on the potential benefits of cardiac myosin inhibitors as a targeted therapeutic approach for HCM.

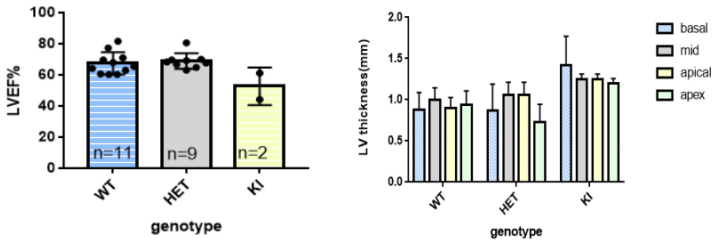

Figure 1

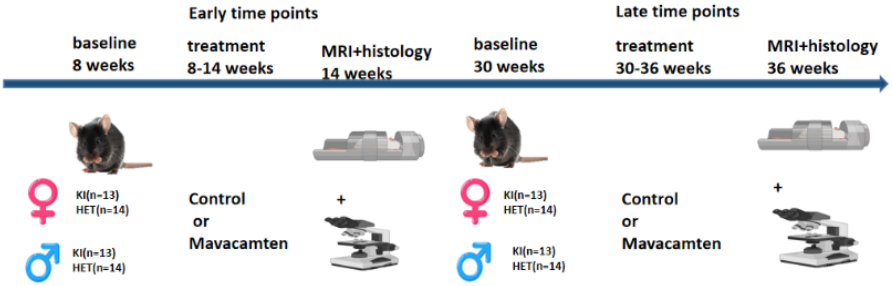

Figure 2

Picture description

Figure1. Different genotype has different LVEF and LV thickness. HCM mice have less LVEF and more LV thickness($P<0.05$).LVEF: Left ventricular ejection fraction. HET:Heterozygous. WT: Wild-type. KI: Gene knock-in.

Figure2. Overview of the Experimental Design for Drug Treatment in HCM Mice. Our study aims to investigate the effectiveness of the cardiac myosin inhibitor in hypertrophic cardiomyopathy (HCM) mice through a comprehensive evaluation of imaging and histological changes before and after early (8 weeks) and late (30 weeks) treatment.

P7

Monitoring of timed degradation of biodegradable metal implants: how MRI can contribute.

Martin Meier[1], *Diane Haake*[1], *Christina Yiannakou*[1]

[1] *ZTL Imaging-Center, Hannover Medical School, Carl-Neuberg-Straße 1, 30625 Hannover, Germany*

Biodegradable metals like magnesium alloys are promising implant materials supporting bone regeneration and avoiding additional surgery to remove implants. Different patient groups and implant applications need different degradation rates not to interfere with tissue regeneration. Animal models are supporting the design of specialized alloys and give parameters for translation, yet not available in cell based testing systems. Imaging with unique modalities like MRI and USPA can extract crucial parameters for implant development, design optimization and patient safety assurance together with 3R fulfillment of the European Directive 2010/63/EU. Here we show unique data and the application of non-invasive imaging in a small animal model of implant degradation to ensure patient safety.

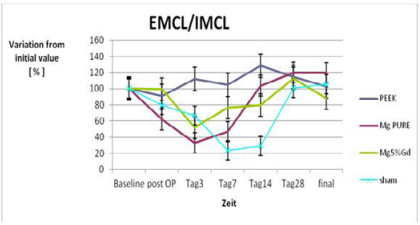

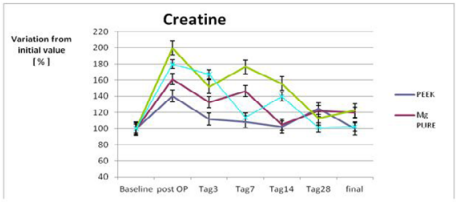

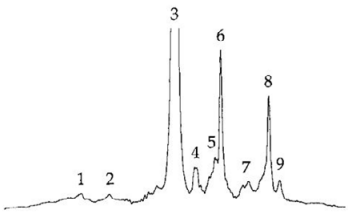

1,2 Carnosine,
3 Water,
4 tCr Methylen Protons,
5 TMA,
6 tCr Methyl Protons,
7-9 Lipids
TMA= trimethyl ammonium-containing compounds

Picture description

Spectroscopy near metal implants

P8

Development and evaluation of kT-point pulses for cardiac magnetic resonance imaging at 7T

Sophia Nagelstraßer[1], *Nico Egger*[1], *Michael Uder*[1], *Armin M. Nagel*[1,2]

[1]*Institute of Radiology, University Hospital Erlangen, Friedrich-Alexander-Universität Erlangen-Nürnberg (FAU), Erlangen, Germany*

[2]*Division of Medical Physics in Radiology, German Cancer Research Centre (DKFZ), Heidelberg, Germany*

Introduction

To mitigate B1+ inhomogeneities that occur at higher magnetic field strengths (B0≥7T), the concept of parallel transmission (pTx) was introduced. Excitation non-uniformities are very pronounced in the human body, requiring dynamic pTx pulses to counteract this problem. kT-point pulses have already proven to benefit the flip angle (FA) homogenization in cardiac MRI at 7T [1]. Pre-computed universal pulses (UP) have shown to improve the excitation uniformity without the need of additional calibration. In this work, these approaches were investigated for our 8Tx/16Rx coil setup.

Methods

3D channelwise, relative B1+ maps [2] of the human heart of 35 healthy subjects (12 female & 23 male, 22-62 years, 16.4-32.2 kg/m^2) were acquired at 7T and subsequently multiplied by a scaling factor determined from an AFI scan to obtain absolute B1+ estimations [3]. Dynamic tailored and UPs with 1-6 kT-points with a subpulse length of 0.15ms and a gradient blip length of 0.09ms were calculated by minimizing a magnitude least-squares problem and evaluated according to their coefficient of variation (CV).

Results

Increasing the number of kT-points results in a reduced median CV for both tailored and universal pulses (Fig.1). For a fixed number of k_T-points, tailored pulses perform better than UPs optimized with the full library. For both pulse types, 4kT-points provide a good trade-off between performance, pulse duration and applied energy dose. Compared to the NullShim with a median CV of 42.1% and the vendor provided cardiac shim with 29.1% for all 35 B1+data sets, the median CV of the tailored 4kT-point pulses is reduced to 5.3% (Fig.2). UP35-4kT achieves a median CV of 10.2%. In vivo measurements of an unseen subject show good results in the context of image quality and contrast and confirm the theoretical predictions (Fig.3).

Discussion

Tailored and universal kT-point pulses improve the FA homogeneity within the human heart at 7T for all 35 B1+data sets. Although a different coil setup and pTx system was used, the results of Aigner et al. [3] could be reproduced.

References

[1] Aigner et al. Magn Reson Med 87.1 (2022): 70-84.

[2] Van de Moortele et al. Proc Intl Soc Mag Reson Med 17 (2009): 367.

[3] Dietrich et al. Magn Reson Med 85.5 (2021): 2552-2567.

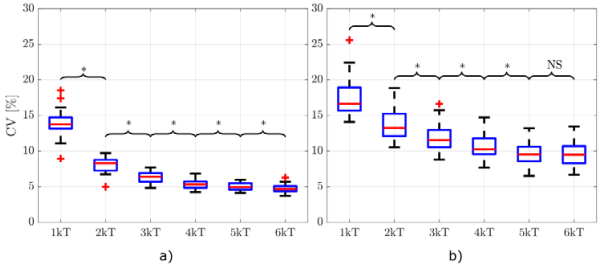

Figure 1

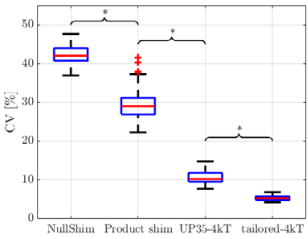

Figure 2

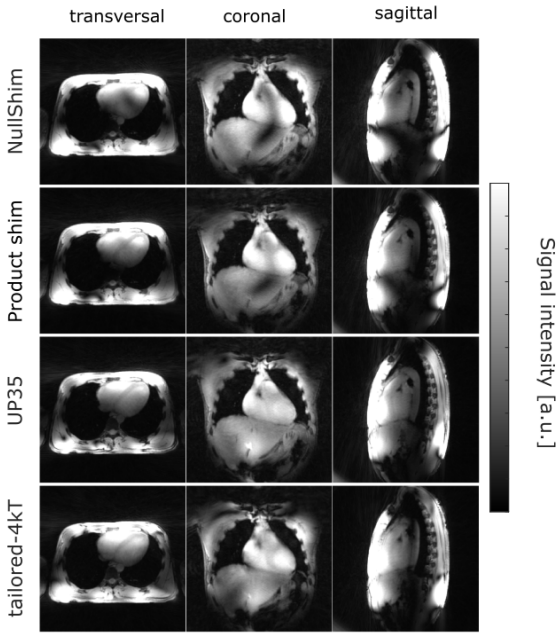

Figure 3

Picture description

Fig.1: Performance of tailored (a) and universal pulses (b) with 1-6 kT-points evaluated on all 35 B1+ data sets. With increasing number of k_T-points, the median CV reduces. For 5 and 6 k_T-points only a slight improvement is observed compared to the 4kT-point pulses. The results, which are statistically significant ($p<0.05$) are marked with a star symbol and not statistically significant results are denoted by “NS”.

Fig.2: Comparison of the performance of the NullShim, the vendor provided cardiac shim, the universal 4kT-point pulse (UP35-4kT) and the tailored 4kT-point pulses. Whereas both shims yield large CV values above 20%, the UP35-4kT reduces the median CV to 10.2%. The tailored pulses result in the lowest CV values for all 35 B1+ data sets with a median CV of 5.3%.

Fig.3: 3D images acquired with a density adapted 3D radial sequence with NullShim, the vendor provided cardiac shim, the pre-optimized universal pulse (UP35-4kT, target FA = 5°) and one tailored-4kT pulse for one unseen subject. While the NullShim and Vec14 yield large signal drop-outs within the heart, the tailored-4kT pulse and the UP35-4kT pulse reduces the problem of RF field inhomogeneities.

P9

Phase Contrast MRI at 7.0 T Improves Near-Wall Hemodynamic Parameters Quantification in Intracranial Aneurysms

Antoine Sache[1], *Philippe Reymond*[2], *Olivier Brina*[2], *Bernd Jung*[3], *Mohamed Farhat*[1], *Maria Isabel Vargas*[2]

[1]*Department of Mechanical Engineering, Ecole Polytechnique Fédérale de Lausanne, Lausanne, Switzerland*

[2] *Division of Neuroradiology, Geneva University Hospital, University of Geneva, Geneva, Switzerland*

[3] *Department of Diagnostic, Interventional and Paediatric Radiology, Inselspital, Bern University Hospital, University of Bern, Bern, Switzerland*

Predicting the risk of rupture of intracranial aneurysms (IAs) is of great interest since this pathology carries a mortality risk of around 30-40% after subarachnoid hemorrhage (SAH). Apart from the classical morphological features (size, location, wall irregularity) used for decision making in daily clinical practice, it has been shown that near-wall hemodynamics parameters, particularly wall shear stress (WSS) and its derived spatiotemporal parameters, are correlated with IAs rupture.

Their measurement, based on knowledge of both the blood velocity field and the location of the arterial walls, is usually achieved using phase-contrast magnetic resonance imaging (PC-MRI). However, their quantification is particularly sensitive to the spatiotemporal resolution of the MRI sequences, which can be limited by low SNR at low field strength or long scan time of 4D flow MRI. Fortunately, the gradual improvement in the signal-to-noise ratio (SNR) of the images over the years, due to the considerable increase in the main magnetic field strength of the MR scanners, has allowed to overcome this issue.

In this work, we demonstrate how ultra-high field (UHF) 7T TOF and PC-MRI sequences coupled with advanced image acceleration techniques enable highly resolved visualization of near-wall hemodynamic parameters patterns along with their accurate quantification inside three in vitro patient-specific IAs models under physiological pulsatile flow conditions.

To this end, we designed an MRI-compatible test bench, which faithfully reproduces a typical physiological intracranial flow rate within the silicone vascular models.

The visualizations revealed high and low WSS patterns with high spatiotemporal resolution (0.5mm and 50ms, respectively) in a reasonable scan time of around 25min. Interestingly, the large oscillatory shear index (OSI) values were found in the core of low WSS vortical structures and in flow stream intersecting regions. In contrast, maxima of WSS occurred around the impinging jet sites.

P10

Evaluation of Dipole Antenna RF Applicators for ThermalMR Theranostics

Nandita Saha[1,2], *Bilguun Nurzed*[1,3], *Thoralf Niendorf*[1,2]

[1] *Max-Delbrück-Center for Molecular Medicine in the Helmholtz Association (MDC), Berlin Ultrahigh Field Facility (B.U.F.F.), 13125 Berlin, Germany*

[2] *Charité—Universitätsmedizin Berlin, Experimental and Clinical Research Center (ECRC), A Joint Cooperation between the Charité Medical Faculty and the Max-Delbrück Center for Molecular Medicine in the Helmholtz Association, 13125 Berlin, Germany*

[3] *Chair of Medical Engineering, Technische Universität Berlin, 10623 Berlin, Germany*

Purpose

Thermal Magnetic Resonance (ThermalMR) is a theranostic concept that combines diagnostic magnetic resonance imaging (MRI) with targeted thermal therapy in the hyperthermia range using an integrated radiofrequency (RF) applicator [1]. ThermalMR efficacy such as uniform B_1^+ for MRI and constructive E-field focusing in the target volume (TV) for thermal therapy is governed by the design of the RF applicator. In this work, we examined the performance of dipole antenna configurations for ThermalMR theranostics of deep-seated brain tumor at 7.0 T.

Methods

EMF simulations (CST Studio Suite 2020) were performed on the human voxel model 'Duke' [1] with an intracranial spheroid tumor TV modification (radius = 2cm, volume=33.5ml[1], σ_{tumor} = 1.15 S/m, ε_{rtumor} = 66.5) (Fig. 1A). The RF applicator cir_HS_SGBT comprises eight compact SGBT[2] dipole antennas (size: 42.3x46.3x2.5 mm^3) and RF applicator cir_HS_FD comprised of eight Fractionated[3] Dipole (FD) (size: 316x40x1.6 mm^3) (Fig. 1 B,C). Both RF applicator configurations are horse-shoe shape (arc=270^0) circular arrays to support MRI at 300 MHz (B_0 = 7.0 T) (Fig. 1C). A Multi-Vector Field Shaping[4] algorithm was used in the time-multiplexing mode to provide phase and amplitude setting for each RF channel to focus SAR_{10g} in the TV and to reduce RF exposure to healthy tissues. The focusing abilities of the RF applicators were evaluated using the metrics SAR_{10g} in TV. Postprocessing was conducted in MATLAB 2020.

Results

The cir_HS_FD configuration provided improved B_1^+ efficiency and homogeneity over the whole brain compared to the cir_HS_SGBT configuration due to larger field of view (Fig. 1D) in circular polarization (CP) mode. However, the cir_HS_SGBT array achieved higher mean and maximum of B_1^+ inside ROI placed in the center of the brain (Fig. 1D). The cir_HS_SGBT array showed a stronger SAR_{10g} focus inside the tumor (Fig. 1E)

while the cir_HS_FD array failed to achieve focal SAR_{10g} targeting inside the tumor. Instead, the SAR_{10g} increase was spread across the entire brain despite using three excitation modes for time-multiplexing (Fig. 1E).

Conclusion

Our findings show that the cir_HS_SGBT RF applicator can form a stronger SAR focus in the tumor than the cir_HS_FD RF applicator. Our findings highlight that SGBT dipole antenna arrays benefit RF power deposition inside the tumor TV and are suited for Thermal MR theranostics.

References

1. Saha, N; Cancers 2023, 15, 2303.
2. Eigentler TW, Magn Reson Med. 2016 Mar;75(3):1366-74.
3. Raaijmakers AJ. Magn Reson Med. 2016 Mar;75(3):1366-74.
4. Kuehne A;Cancers. 2020; 12(5):1072.

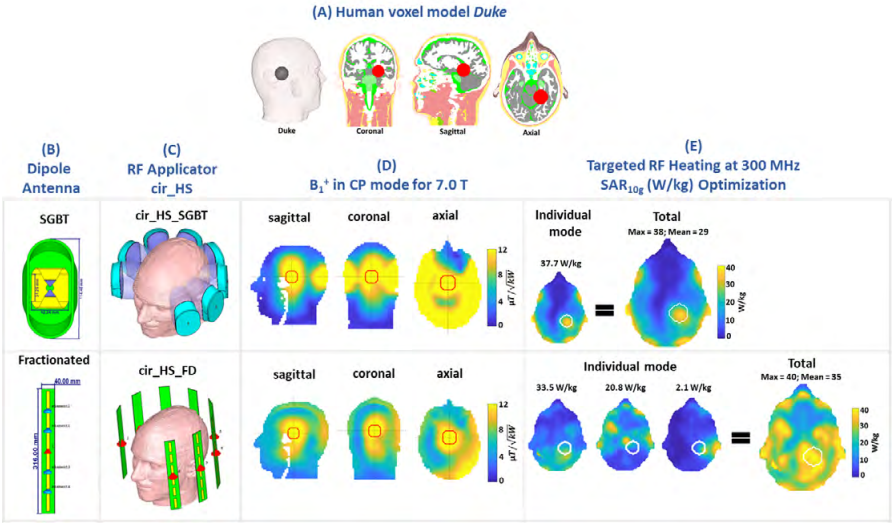

Picture description

Figure 1. (A) Human voxel model 'Duke' from the virtual family IT'IS modified with a small brain tumor (red) in the right parietal region. (B) Dipole antenna element: Self Grounded Bow-Tie (SGBT) dipole building block (top); Fractionated Dipole (bottom) with inductor of 33.5nH as lumped element 1-4. (C) ThermalMR RF applicators cir_HS_SGBT and cir_HS_FD placed around Duke's head. (D) B1+ distribution maps of Duke's head for cir_HS_SGBT and cir_HS_FD ThermalMR RF applicators at 7.0 T in circular polarization (CP) mode with a center ROI (red circle). (E) Targeted RF heating SAR10g optimization in time-multiplexing mode. Targeted tumor region is highlighted by the white line. The larger plots on the right side shows the total achieved SAR10g in the tumor TV. The resultant target pattern was created from the individual contributing time-multiplexed modes scaled to their individual maxima, shown in the smaller plots on the left sides.

P11

A Triple CycleGAN Model Ensemble for Motion Correction in 7T MR Brain Images

Gulfam Ahmed Saju[1], *Huy Anh Pham*[2], *Yuchou Chang*[1]

[1] *Department of Computer and Information Science, University of Massachusetts Dartmouth, North Dartmouth, MA 02747, USA*

[2]*Intelligent Medical Objects, Inc., Houston, Texas, USA 77021*

Proposed Method

In this abstract, we introduce an innovative method for motion correction in MRI images using an ensemble of three CycleGAN [1] models. Each model is trained on different motion-corrupted high-field 7T MRI brain data. Three separate CycleGAN models are trained with different types of motion-corrupted MRI brain data. Each model comprises two generators and two discriminators, which translate and distinguish between motion-free and motion-corrupted images. The key to the approach is the ensemble operation of the three trained CycleGAN models. This ensemble operation averages the output of each model to improve robustness and overall performance. The output of this ensemble operation is then used to transform a given motion-distorted MRI image into a motion-free image.

The implementation of this method involved the training of three distinct CycleGAN models using unique high-field 7T fMRI T1-weighted datasets [2] of brain images. Motion-corrupted brain images are simulated using a comprehensive motion simulation tool named View2DMotion [3] package. The Adam optimizer was employed with a learning rate of 0.0002, beta-1 set to 0.5, and beta-2 set to 0.999. The models were trained for 200 epochs using a blend of adversarial loss, cycle consistency loss, and identity loss.

After the completion of training, each CycleGAN model can transform a motion-corrupted image into a motion-corrected image. During the experiment, a motion-corrupted image is fed into each model to get a motion-free image. Following this, an ensemble operation synthesizes the outputs from all models. This collective approach results in a final output image with superior motion correction than a single CycleGAN model. The effectiveness of our method was validated through a comprehensive evaluation involving multiple brain slices.

References

[1]. Zhu, J. Y., Park, T., Isola, P., & Efros, A. A. (2017). Unpaired image-to-image translation using cycle-consistent adversarial networks. In Proceedings of the IEEE international conference on computer vision (pp. 2223-2232).

[2]. High-field 7T Visual fMRI datasets. https://openneuro.org/datasets/ds002702/versions/1.0.1.

[3]. Lee, S., Jung, S., Jung, K. J., & Kim, D. H. (2020). Deep learning in MR motion correction: a brief review and a new motion simulation tool (view2Dmotion). Investigative Magnetic Resonance Imaging, 24(4),

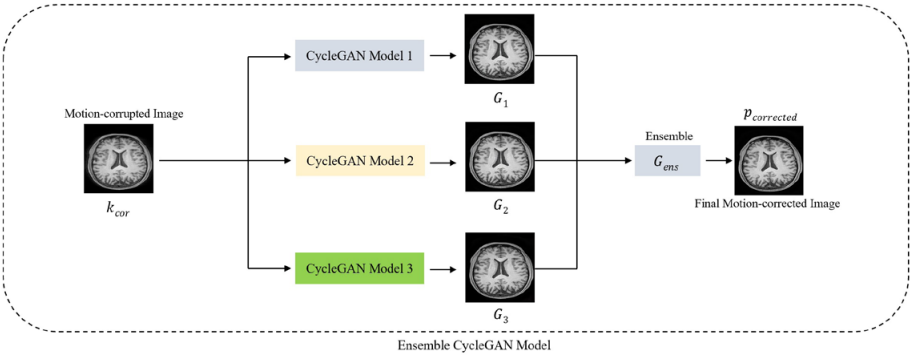

Figure 1

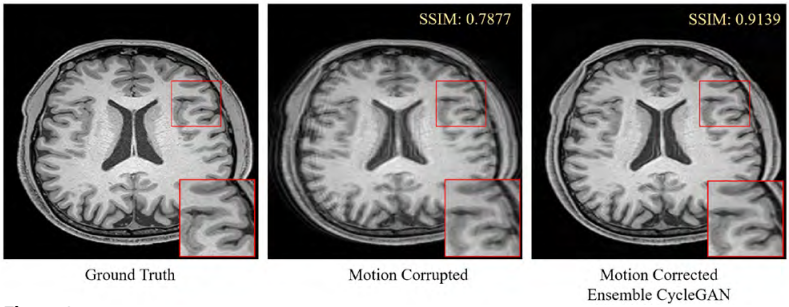

Figure 2

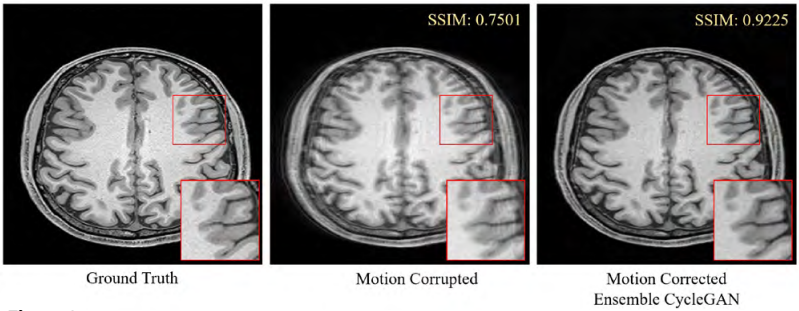

Figure 3

Picture description

Figure 1: The diagram illustrates how the Ensemble CycleGAN method transforms a motion corrupted image into motion-corrected one.

Figure 2: Motion correction results for first MRI brain slice. The three brain images are respectively, (a) Ground truth image; (b) Motion-corrupted image with SSIM=0.7877; (c) Motion-corrected image using the ensemble CycleGAN method, significantly improved with SSIM=0.9139.

Figure 3: Result of motion correction for the second brain slice. The three brain images are respectively, (a) Ground truth image; (b) Motion-corrupted image with SSIM=0.7501; (c) Motion-corrected image using the ensemble CycleGAN method, significantly improved with SSIM=0.9225.

P12

Advanced Cardiac MRI: Catching Heart Motion with Free-Running 3D Whole-Heart T2* mapping in Hypertrophic CardioMyopathy (HCM) model

Shahriar Shalikar[1], Archana Malagi[2], Hsin-Jung Yang[2], Oumaima Laghazli[1], Thoralf Niendorf[1,3,4], Min-Chi Ku[1,3]

[1]*Berlin Ultrahigh Field Facility (B.U.F.F.), Max Delbrueck Center for Molecular Medicine in the Helmholtz Association, Berlin, Germany*

[2]*Biomedical Imaging Research Institute, Cedars-Sinai Medical Center, Los Angeles, CA, United States*

[3]*DZHK (German Centre for Cardiovascular Research), partner site Berlin, Germany*

[4]*Experimental and Clinical Research Center, Charite Medical Faculty and the Max Delbrueck Center for Molecular Medicine in the Helmholtz Association, Berlin, Germany*

Introduction

Changes in myocardial T2* can indicate tissue alterations, such as edema or fibrosis, providing valuable insights into heart conditions, including cardiomyopathies and heart failure [1]. However, the conventional ECG-gated, Multi-Gradient-Echo (MGE) T2* approach suffers imperfect ECG-gating due to switching of magnetic field generated by the gradient coils. This issue becomes even more challenging in mouse models, where the high heart rate restrains data acquisition time, and faster gradient switching is required for MGE. To address these challenges, we developed a motion resolved, time-efficient, fully ungated, 3D T2* mapping approach at 9.4T Bruker scanner. The acquired data are reconstructed using a Low-Rank Tensor (LRT) framework, which helps to mitigate motion-related issues and improves the accuracy and reliability of T2* cardiac MRI in mice models.

Methods

Data Acquisition: The Bruker 3D MGE sequence has been modified in order to change conventional cartesian phase-encoding (PE) to 2D randomized gaussian distribution [2] (Figure 1). Dense samples in the center of k-space enables higher SNR and more efficient sampling compared with conventional Cartesian ordering. To determine the amount of motion, an additional zero-encoded acquisition (k-space center line) has been added as a navigator in an interleaved manner (blue line in middle illustration of Figure 1). Data acquisition was performed continuously throughout the cardiac and respiratory cycles.

Image Reconstruction: The image, modelled as a 6D low-rank tensor (3 spatial dimensions for each xyz and 3 temporal dimensions for Cardiac, Respiratory and T2* evolution), were reconstructed based on MR Multi-Tasking approach [3] (Figure 1). To ensure that the proposed sequence has been developed correctly, a phantom study have been also done and its image reconstructed by Non-Uniform FFT technique.

Results & Discussion

To evaluate the proposed approach, a phantom study was performed (Figure 2). The resulting ghosting artifact in the PE direction is due to unequally-spaced sampling and smaller number of PE in the phantom study. Figure 3 shows the LRT reconstruction of an in vivo scan of mice heart with imaging parameters summarized in Table 1. Our preliminary findings show an image quality free of major motion artifacts, which facilitate the calculation of T2* map.

References

[1]. Gastl, et al., Elsevier 2019; [2]. Guan et al. ISMRM 2023; [3]. Christodoulou et al., Nature 2018.

Long reference

[1] M. Gastl *et al.*, "Cardiovascular magnetic resonance T2* mapping for structural alterations in hypertrophic cardiomyopathy," *European journal of radiology open,* vol. 6, pp. 78-84, 2019.

[2] X. Guan *et al.*, "Free-breathing Fully Ungated 3D Cardiac T2* MR Mapping using a Low-Rank Tensor Framework."

[3] A. G. Christodoulou *et al.*, "Magnetic resonance multitasking for motion-resolved quantitative cardiovascular imaging," *Nature biomedical engineering,* vol. 2, no. 4, pp. 215-226, 2018.

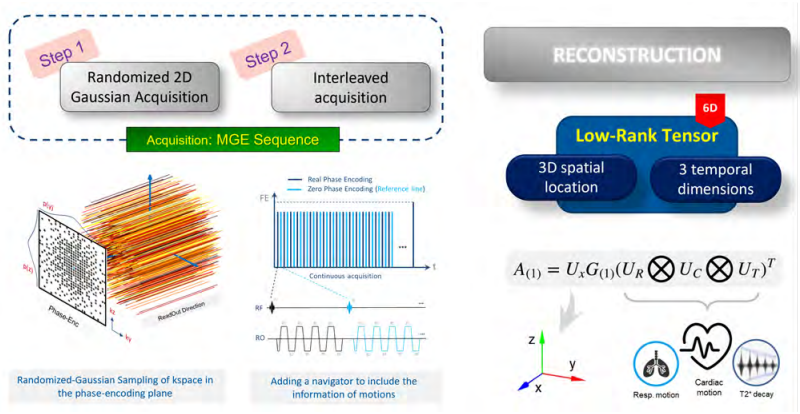

Figure 1

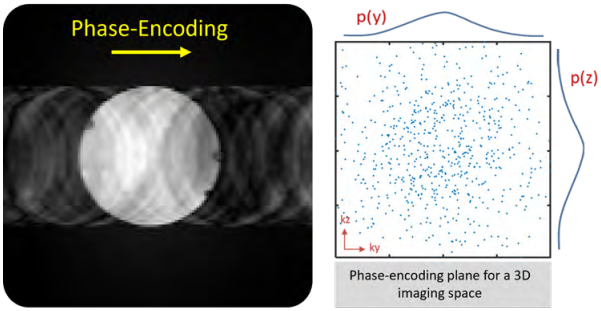

Figure 2

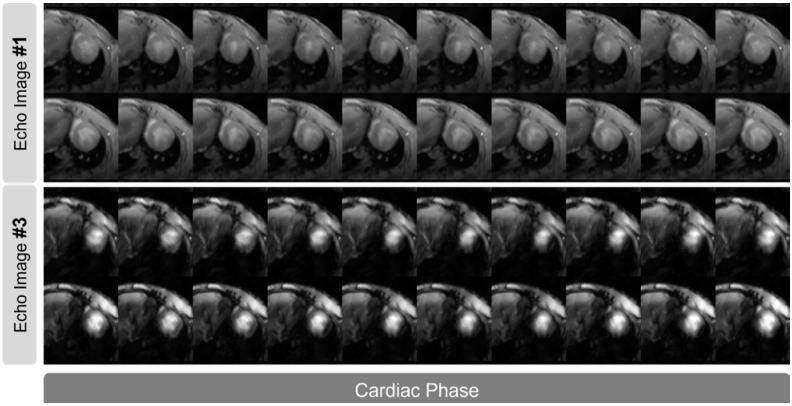

Figure 3

Parameters	Value
TE (ms)	1.5, 2.72, 3.94, 5.16, 6.38, 7.60
TR (ms)	10
FOV (mm)	30x30x10
Matrix Size	128*128*16
FA (°)	10°
Number of Repetition	25 (*in vivo*), 1 (Phantom)
Scan time	08m53s333ms (*in vivo*) 20s48ms (phantom)

Table 1

Picture description

Figure 1. An Overview of Low-Rank Tensor approach for free-breathing ungated Quantitative MRI. The acquisition is a 3D MGE, which a randomized-gaussian distribution was performed in the 2D phase-encoding plane. Concentrated samples in the center of kspace leads to higher Image SNR. A reference acquisition with zero phase-encoding (blue line of sequence in the middle illustration) also added after each real phase-encoding to take motion information into account for the reconstruction step. The LRT reconstruction framework models the acquired data as a 6D tensor with 3 spatial, and 3 temporal dimensions reflecting Cardiac motion, Respiratory motion and T2* relaxation decay respectively. MGE: Multi -Gradient-Echo, LRT: Low-Rank Tensor.

Figure 2. Phantom experiment result. The image was reconstructed by NUFFT technique according to the randomized 2D gaussian-pattern phase-encoding ordering shown on the right figure. The introduced ghosting artifact is due to variable-distance sampling in the PE direction.

Figure 3. Primary result of multi-echo images of mice heart at mid-SAX view reconstructed by LRT framework for 10 cardiac phases. SAX: Short-Axis View

Table 1: Imaging parameters for Phantom and in vivo scanning.

P13

Toward Assessment of Renal Tubule Volume Fraction in Rat Kidney Using Decomposition of Parametric T2 Mapping

Ehsan Tasbihi[1], *Thomas Gladytz*[1], *Ludger Starke*[1,2], *Jason M. Millward*[1], *Erdmann Seeliger*[3], *Thoralf Niendorf*[1,4]

[1] *Berlin Ultrahigh Field Facility (B.U.F.F.), Max Delbrueck Center for Molecular Medicine in the Helmholtz Association, Berlin, Germany*

[2] *Hasso Plattner Institute for Digital Engineering, University of Potsdam, Germany*

[3] *Institute of Translational Physiology, Charité – Universitätsmedizin Berlin, Berlin, Germany*

[4] *Experimental and Clinical Research Center, a joint cooperation between the Charité Medical Faculty and the MAX Delbrück Center for Molecular Medicine in the Helmholtz Association, Berlin, Germany*

Increased incidence of kidney diseases is a substantial global concern and current biomarkers and existing treatment options are unsatisfactory. Changes in renal tubule luminal volume fraction (TVF) is a potential rapid biomarker for kidney disease. T2 mapping is an established MRI technique that can be used for quantifying changes in the tissue water fraction in vivo, and may provide a tool to probe renal tissue properties noninvasively. The ultimate aim of this work is to determine the TVF in the rat kidney from MRI using T2 mapping, by applying multiexponential analysis of the T2 driven signal decay.

Methods

The numerical solution for multi-exponential decomposition was done using MATLAB functions. The algorithm was evaluated using synthetic data simulations and measurements in phantoms. A 2-compartment-model developed based on Bloch-simulations. MRI data were acquired with a 2-channel volumetric transceiver RF coil on a 9.4T animal MR scanner (Bruker). T2 mappings was MESE-techniqueResultsWe provide Mean Absolute Error (MAE) measuring TVF acquired with for multi-exponential decomposition, using the dictionary of distributed T2s with echo spacing, varying volume fractions, number of echoes and flip angles. Figure1 shows a visualization of the reconstructed maps of the custom-built T1-T2 phantom; the histogram shows the T2 distribution corresponding to the selected exemplary ROI. An accuracy of 98% (Table2) was achieved with modified Trust-Region on the phantom

Conclusion

Our preliminary results demonstrate that modified Trust-Region is promising for research into quantitative assessment of renal TVF in in vivo applications. Future in vivo experiments with physiologically relevant interventions (e.g. increased pressure in the renal pelvis and tubules) for altering TVF is required to further study these methods. Future validation of this MR approach with intravital microscopy, i.e. for quanti-

tative comparison of changes in the vascular and renal tubular compartments with those observed by T2* and T2, is also warranted. Ultimately, these investigations have the potential to help uncover the hidden patterns in acute renal injury that lead to chronic kidney disease, which will improve diagnosis, prognosis and treatment of renal disorders.

$x = \frac{S_w}{S_w + S_d}$	estimated (optimal protocol)	estimated (in vivo protocol)
15%	14.48%	13.29%
17%	16.44%	16.48%
20%	19.38%	21.1%
25%	24.29%	28.43%
33%	32.18%	39.27%
50%	49.06%	59.23%
66%	65.03%	74.99%

Picture description

Assessment of Renal Tubule Volume Fraction in Rat Kidney Using Decomposition of Parametric T2 on mechanical phantom. Estimated tubule volume fraction obtained for the study phantom with optimal protocol was acquired with scan parameters TR = 4 s, number of echoes = 15, first TE = 10 ms, interecho time ΔTE = 10 ms, number of averages = 3. x= expected fraction, Sw= Surface of water, Sd= Surface of doped water. Estimated tubule volume fraction obtained for the study phantom with in vivo protocol was acquired with scan parameters TR = 1 s, number of echoes = 13, first TE = 6.4 ms, interecho time ΔTE = 6.4 ms, number of averages = 1, tacquisition = 58 s.

P14

Advancing 7T BOLD fMRI Spatial Accuracy and Sensitivity: Unveiling Individual Brain Neurosignatures

Igor F. Tellez Ceja[1,3], *Thomas Gladytz*[1], *Ludger Starke*[1], *Karsten Tabelow*[2], *Thoralf Niendorf*[1,3], *Henning M. Reimann*[1]

[1] Berlin Ultrahigh Field Facility (B.U.F.F.), Max Delbrück Center for Molecular Medicine in the Helmholtz Association, Berlin, Germany

[2] Weierstrass Institute for Applied Analysis and Stochastics, Berlin, Germany

[3] Experimental and Clinical Research Center, a joint cooperation between the Charité Medical Faculty and the Max Delbrück Center for Molecular Medicine in the Helmholtz Association, Berlin, Germany

Introduction

High sensitivity and spatial accuracy are crucial for detecting BOLD fMRI effects at UHF. Denoising methods increase sensitivity at the cost of losing spatial accuracy. Using synthetic fMRI data, Gaussian, spatially adaptive nonlocal averaging (SANLM), and adaptive weight smoothing (AWS) filters were evaluated. BOLD sensitivity and spatial accuracy metrics ranked the performance of the filters. A new metric was introduced to measure filter impact on BOLD magnitude. The objective is to evaluate a suitable method to maintain BOLD pattern accuracy with high sensitivity.

Methods

Synthetic data sets: created from an experimental fMRI time series volume (spatial resolution=1.5 mm isotropic). Four masks with different shapes and sizes were designed to define the activation regions with different magnitudes; homogeneous, 6% and heterogeneous, mixing 1.5%, 3% and 6% (Fig. 2a). Three noises were simulated, Gaussian, Rician and “acquired” which mainly consisted of thermal noise. The noises were amplified at 1%, 2% and 4%, to which tSNR corresponds to a cortical and subcortical region of a real fMRI dataset. Gaussian smoothing kernels: 1x, 1.5x and 2.5x voxel size. SANLM filtering: light, medium and strong intensities. AWS at its default filtering values. Spatial accuracy: Sørensen-Dice coefficient formula (Fig.3a). BOLD sensitivity: true positives (TP) divided by the sum of TP and false negatives (Fig. 3b). RSM: correlation coefficient between ground truth and parameter estimates masked with the z-map of activity (Fig. 2b).

Results

Gaussian and SANLM filters amplified the BOLD effect but blurred the spatial details of BOLD clusters and deformed the original shapes of the clusters (Fig. 1). AWS maintained the geometry of BOLD clusters at noise levels in the cortical tSNR range. AWS achieved substantially higher accuracy at the first three noise levels. BOLD sensitivity was approximately similar across filters (Fig. 3a-b). AWS preserves the original sig-

nal better than other filtering methods. (Fig. 2b). AWS got the best results in terms of overall accuracy, with comparatively high sensitivity and significantly higher RSM scores (Fig. 3c).

Discussion & Conclusion

AWS is a superior filtering method that boosts BOLD sensitivity while preserving spatial accuracy and depicting the best fidelity of the activations. Our finding provides an essential technical foundation for correctly analyzing BOLD fMRI into fine-grained functional neurosignatures

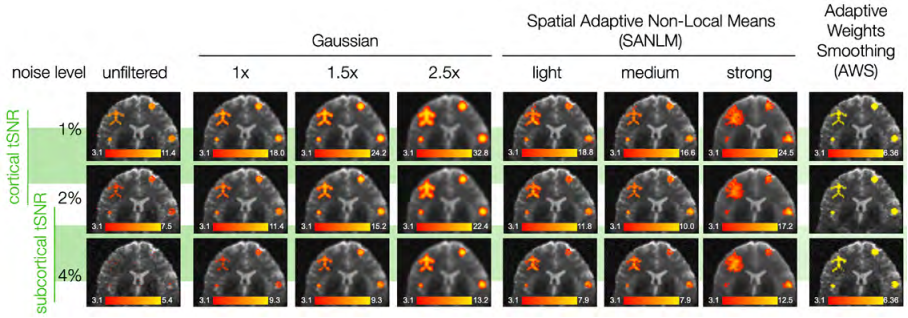

Figure 1

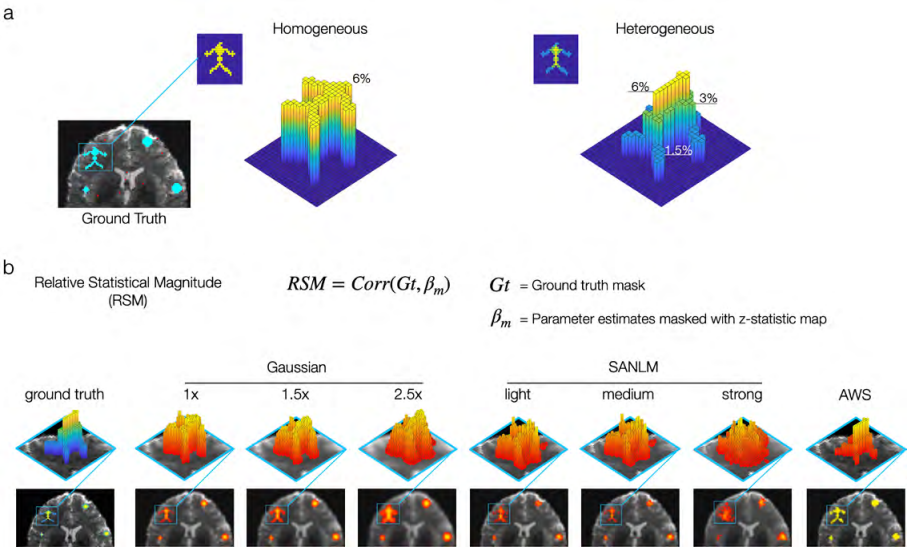

Figure 2

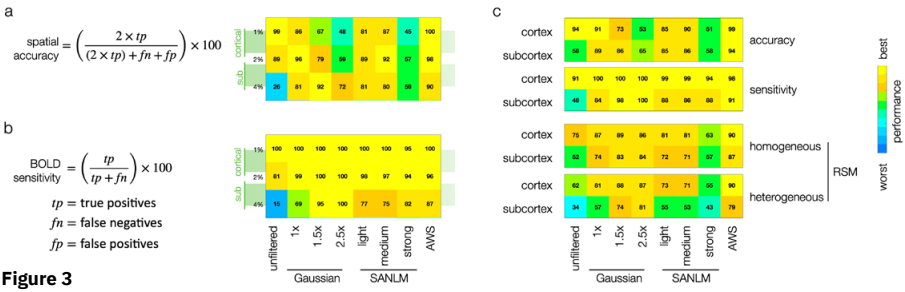

Figure 3

Picture description

Figure 1. BOLD cluster comparison: Gaussian noise between 1-4% noise levels. Unfiltered data compared to Gaussian, SANLM, and AWS filters. Gaussian filters amplify the BOLD effect but blur the spatial details of BOLD clusters. SANLM data show an enlargement of BOLD activity, deforming the shapes of the original clusters. AWS preserves the geometry of the cluster at the cortical tSNR range. Gaussian and SANLM filter z-scores decrease at 4% of noise. AWS keeps the same degree of z-scores along all the noise levels, depicting all the BOLD clusters with their highest value (6.36).

Figure 2. a) The used BOLD magnitude was homogeneous across all ground truth masks at 6%. To model more realistic activations, we designed heterogeneous activations with 3 different magnitude levels, 1.5%, 3%, and 6%. b) Besides evaluating the spatial accuracy and sensitivity, we decided to investigate the effects of the filters on BOLD signals by designing a metric named Relative Statistical Magnitude (RSM). RSM measures the correlation coefficient between the ground truth and the parameter estimates, calculated by the general linear model (GLM) delimited by the thresholded activity maps. AWS preserves the original signal better than other filtering methods.

Figure 3. a) Spatial accuracy of time series with Gaussian noise. The amplification effect of Gaussian and SANLM filters produces several false positives, causing accuracy to decrease. AWS achieved the highest accuracy. b) Sensitivity is higher for Gaussian filters but remains high for the other filtering methods. c) Overall results averaged over the three types of simulated noise, and the noise level ranges corresponding to cortical and subcortical regions. AWS obtained the highest spatial and RMS accuracy and considerably high sensitivity.

P15

Rapid PD, T2, and T2* Mapping with 2in1-RARE-EPI and Model-Based Reconstruction in Multiple Sclerosis

Jose Raul Velasquez Vides[1,2], Carl J. J. Herrmann[1,3], Ludger Starke[1,4], Hampus Olsson[1], Georg Rose[2,5], and Thoralf Niendorf[1,6]

[1]*Max-Delbrück-Center for Molecular Medicine in the Helmholtz Association, Berlin Ultrahigh Field Facility (B.U.F.F), Berlin, Germany,*

[2]*Institute for Medical Engineering, Otto von Guericke University,*

[3]*Department of Physics, Humboldt University of Berlin, Berlin, Germany,*

[4]*Digital Health - Machine Learning Research Group, Digital Health Center, Hasso Plattner Institute, University of Potsdam, Potsdam, Germany,*

[5]*Research Campus STIMULATE, Otto von Guericke University, Magdeburg, Germany,*

[6]*Experimental and Clinical Research Center (ECRC), a joint cooperation between the Charité Medical Faculty and the Max-Delbrück-Center for Molecular Medicine in the Helmholtz Association, Berlin, Germany*

Introduction

T2 and T2* mapping are viable imaging markers for monitoring multiple sclerosis (MS)[1-2]. However, they require long acquisition times. Our group developed a radially-sampled 2in1-RARE-EPI technique for simultaneous T2 and T2* mapping in MS patients[3]. Model-based reconstruction (MBreco) is conceptually appealing for estimating MR parameters from undersampled data[4-5]. This work combines 2in1-RARE-EPI with MBreco to accelerate the estimation of PD, T2, and T2* maps. Our results demonstrate a synergistic effect, resulting in reduced acquisition times.

Methods

Experiments were performed on a SkyraFit 3T system using a 32-channel coil (FOV 232x232 mm2, matrix size 256x256, excitations=200, TR=2000 ms, bandwidth=610 Hz/pixel, ETL=14/18, ESP=6.5/2.3 ms). For validation, standard multi-echo spin-echo (MSE) and multi gradient-echo (MGRE) techniques were used, with geometries and timings identical to the 2in1-RARE-EPI acquisitions. Firstly, TE images were reconstructed using BART[6]. Then, pixelwise fitting of the magnitudes of the TE images (2in1-RARE-EPI, MSE, MGRE) was performed to obtain T2 and T2* maps. Secondly, the 2in1-RARE-EPI data was retrospectively undersampled from 200 to 34 spokes per echo. Then, PD, T2, T2*, and B0 maps were calculated, using the BART implementations of the MBreco strategies[4-5].

Results

Figure 1 shows T2 and T2* maps of a healthy volunteer using the three acquisitions and the two mapping methods. The adoption of the MBreco methods for 2in1-RARE-EPI provides comparable results to the pixelwise fitting approach while dramatically

decreasing acquisition time. Figure 2 shows T2 and T2* maps of an MS patient. The mean and standard deviations obtained for an ROI (7x7 pixels) covering the MS lesion reveal that 2in1-RARE-EPI with MBreco allows for correct quantification.

Discussion

This work shows that the acquisition time of 2in1-RARE-EPI can be drastically reduced (01:40 min vs 07:12 min) using MBreco, without affecting image quality. Our work provides a technical foundation to support the implementation of quantitative mapping in routine practice, and for conducting broader clinical studies. The potential range of clinical applications for MBreco 2in1 RARE EPI for T2 and T2* mapping extends well beyond MS to several other pathologies in the brain and other target organs.

References

1.Bonnier, ACTN 2014; 2.Blazejewska, JMRI 2014; 3.Herrmann, MRM 2021; 4.Wang, PTRS 2021; 5.Tan, IEEE 2023; 6.Uecker, ISMRM 2015.

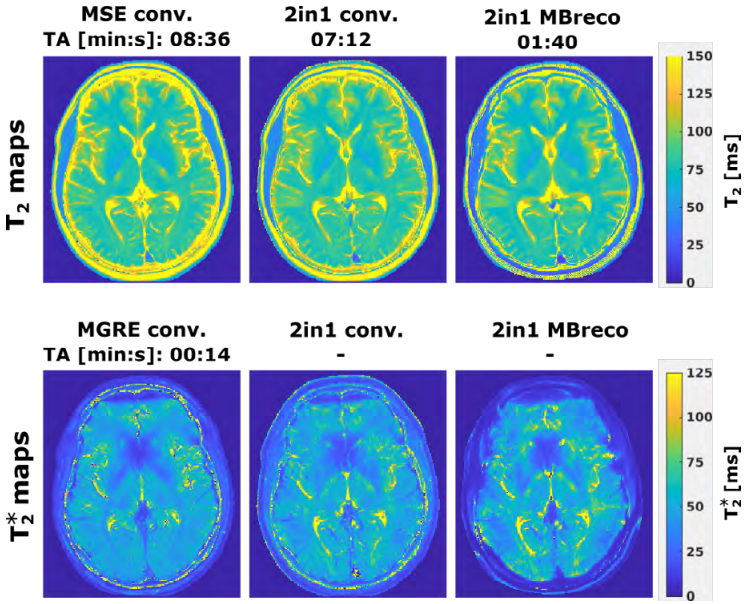

Figure 1

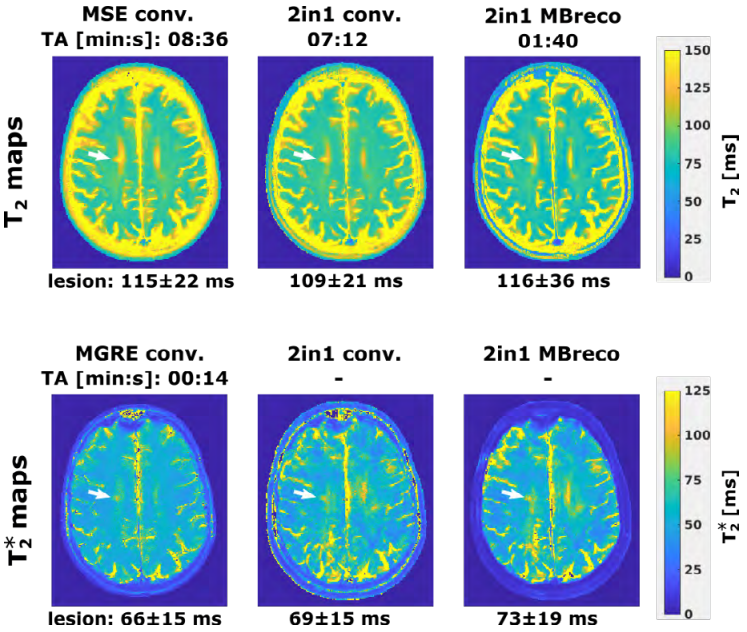

Figure 2

Picture description

Figure 1. T2 and T2* maps of the brain of a healthy subject obtained from the MSE, MGRE (first column), and 2in1-RARE-EPI sequence (middle and last column). The maps from the first two columns were calculated by performing a conventional pixelwise fitting. The maps from the last column were obtained using MBreco methods. Adopting an MBreco approach allows for higher undersampling factors and hence, a substantial reduction of the acquisition time without compromising the quality of the maps. The EPI data is measured during the waiting time of the RARE module.

Figure 2. T2 and T2* maps of an MS patient obtained using the MSE, MGRE (first column), and 2in1-RARE-EPI (middle and last column). The mean and standard deviations obtained for an ROI (7x7 pixels) covering the MS lesion reveal that 2in1-RARE-EPI with MBreco allows for correct quantification.

P16

Study of the radiofrequency-induced heating inside the human head with dental implants at 7 T

Song Duan[1], Xiuxiu Wu [1], Juntian Shi [1], Wenhui Li [2,], Qingshan Dong [3], Sherman* ***Xuegang Xin***[4,*]

[1] *Department of Radiation Oncology, Sun Yat-Sen Memorial Hospital, Sun Yat-Sen University, Guangzhou, Guangdong, China.*

[2] *Air Force Hospital of Southern Theater Command of PLA, Guangzhou, Guangdong, China.*

[3] *Department of Stomatology, General Hospital of Central Theater Command of PLA, WuHan 430070, China.*

[4] *School of Medicine, South China University of Technology, Guangzhou, Guangdong, China.*

[*] *Correspondence to: Wenhui Li, Air Force Hospital of Southern Theater Command of PLA, Guangzhou, Guangdong, China. (E-mail: lwh458@163.com).*
Sherman Xuegang Xin, School of Medicine, South China University of Technology, Guangzhou, Guangdong, China. (E-mail: xinxg@scut.edu.cn).

Conductive dental implants are commonly used in restorative therapy to replace missing teeth in patients. Ensuring the radiofrequency (RF) safety of these patients is crucial when performing 7 T MR scans of their heads. This study aimed to investigate RF-induced heating inside the human head with dental implants at 7 T. Dental implants and their attachments were fabricated and integrated into an anatomical head model, creating different measurement configurations (MCs). Numerical simulations were conducted using a 7 T transmit coil loaded with the anatomical head model, both with and without dental implants. The maximum temperatures inside the head for various MCs were computed using the maximum permissible input powers (MPIPs) obtained without dental implants and compared with published limits. Additionally, the MPIPs with dental implants were calculated for scenarios where the temperature limits were exceeded. The maximum temperatures observed inside the head ranged from 38.4 to 39.6 °C. The MPIPs in the presence of dental implants were 81.9% to 97.3% of the MPIPs in the absence of dental implants for scenarios that exceeded the regulatory limit. RF-induced heating in the dental implants was not significant. The safe scanning condition in terms of RF exposure was achievable for patients with dental implants. For patients with conductive dental implants of unknown configuration, it is recommended to reduce the input power by 18.1% to ensure RF safety.

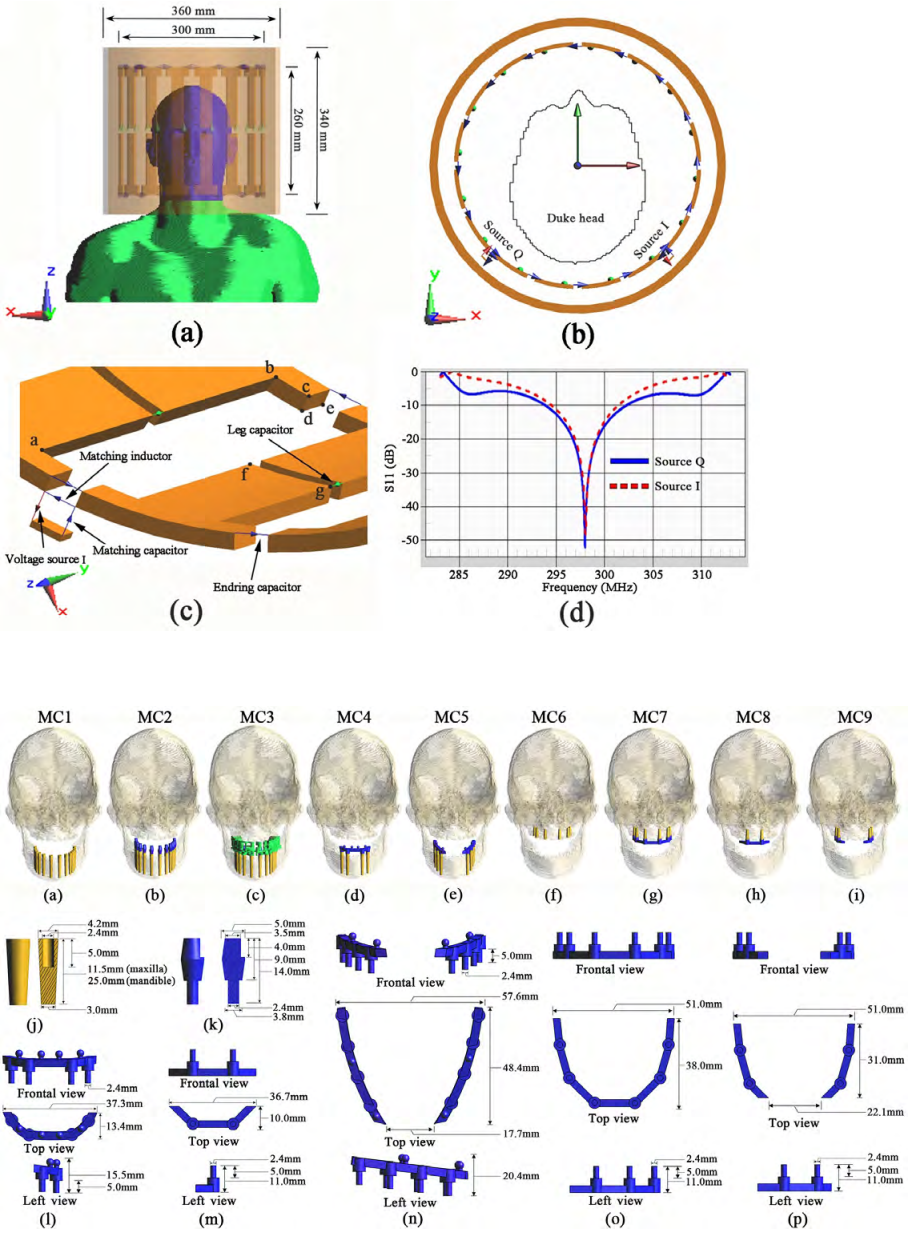
360 mm
300 mm
260 mm
340 mm
(a)
Duke head
Source Q
Source I
(b)
a
b
c
d
e
f
g
Leg capacitor
Matching inductor
Matching capacitor
Voltage source I
Endring capacitor
(c)
S11 (dB)
Source Q
Source I
Frequency (MHz)
(d)
MC1
MC2
MC3
MC4
MC5
MC6
MC7
MC8
MC9
(a)
(b)
(c)
(d)
(e)
(f)
(g)
(h)
(i)
4.2mm
2.4mm
5.0mm
11.5mm (maxilla)
25.0mm (mandible)
3.0mm
(j)
5.0mm
3.5mm
4.0mm
9.0mm
14.0mm
2.4mm
3.8mm
(k)
Frontal view
2.4mm
37.3mm
13.4mm
Top view
15.5mm
5.0mm
Left view
(l)
Frontal view
36.7mm
10.0mm
Top view
2.4mm
5.0mm
11.0mm
Left view
(m)
Frontal view
5.0mm
2.4mm
57.6mm
48.4mm
17.7mm
Top view
20.4mm
Left view
(n)
Frontal view
Frontal view
51.0mm
38.0mm
Top view
2.4mm
5.0mm
11.0mm
Left view
(o)
Frontal view
51.0mm
31.0mm
22.1mm
Top view
2.4mm
5.0mm
11.0mm
Left view
(p)

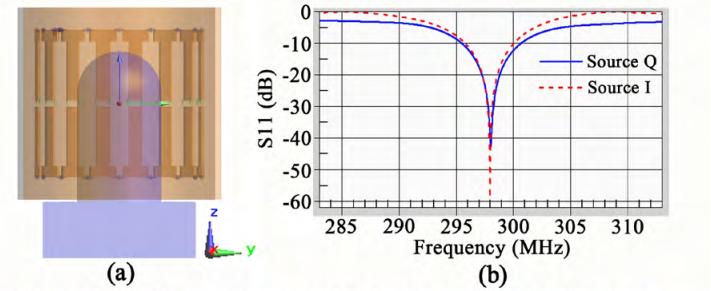
z
y
0
-10
-20
-30
-40
-50
-60
S11 (dB)
285
290
295
300
305
310
Frequency (MHz)
Source Q
Source I
(a)
(b)

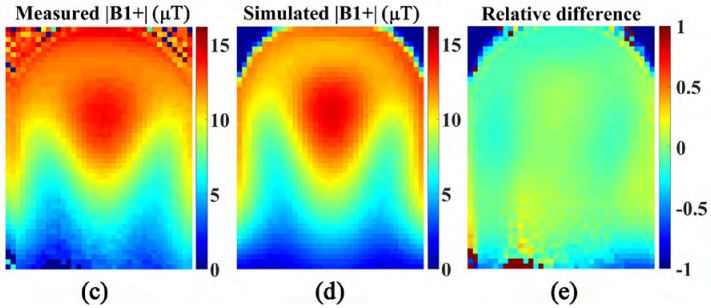
Measured |B1+| (μT)
Simulated |B1+| (μT)
Relative difference
15
10
5
0
1
0.5
0
-0.5
-1
(c)
(d)
(e)

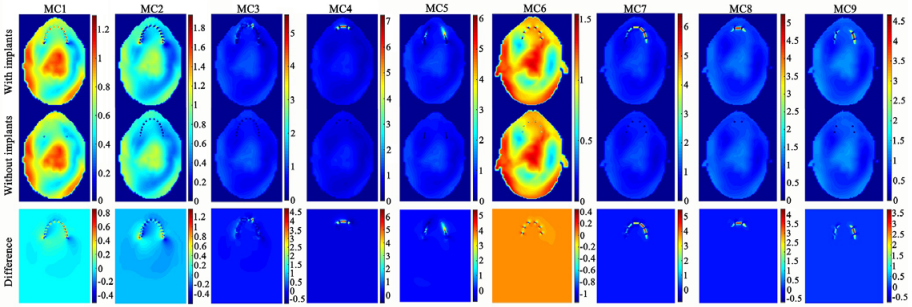
MC1
MC2
MC3
MC4
MC5
MC6
MC7
MC8
MC9
With implants
Without implants
Difference

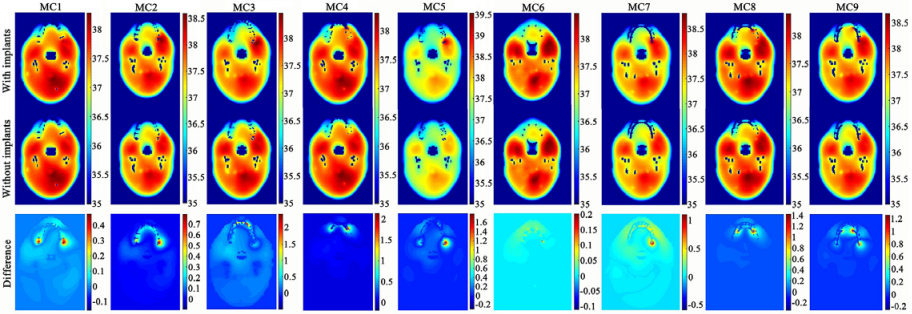
MC1
MC2
MC3
MC4
MC5
MC6
MC7
MC8
MC9
With implants
Without implants
Difference

Flywheel for Core Facilities

Powering Your Imaging Research

Streamline multimodal data capture, curation, processing, and sharing with a scalable data management platform. Flywheel delivers tools that dramatically improve efficiency and service, helping core facilities differentiate their expertise and ensure reproducibility.

Deliver value-added services, improve productivity, and reduce costs

Flywheel is a cloud-based biomedical research data platform that streamlines data capture from multiple sources, curates it to common standards, automates processing and machine learning pipelines, and provides for secure collaboration with internal and external partners.

Flywheel's comprehensive data management platform offers tools for:

Efficient data capture

- Automated DICOM & raw data capture
- PACS and VNA integration
- Integrated de-identification

Quality, consistency and reproducibility

- Automated pre-processing & pipeline execution
- Data quality controls
- BIDS curation and apps
- Comprehensive provenance

Findable and reusable data

- Automated metadata indexing to enable search
- Secure collaboration
- Efficient cohort creation

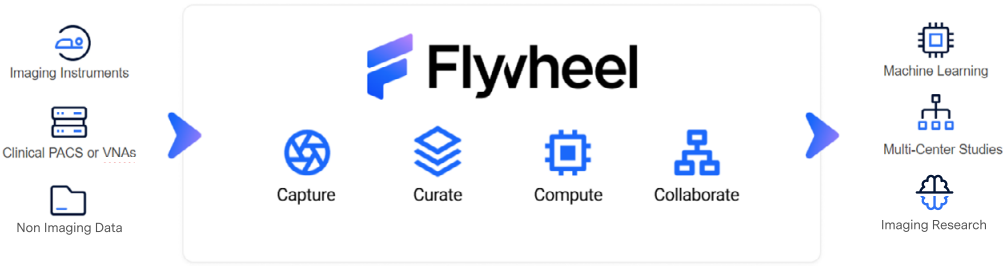

Phone: +1-612-223-7359 | Email: info@flywheel.io | Website: www.flywheel.io | Flywheel

Sponsors

The organizers gratefully acknowledge the symposium's sponsors who provided kind contributions to foster science and educational activities.

www.bruker.com

www.siemens-healthineers.com

www.stiftung-charite.de

www.nvision-imaging.com

flywheel.io

www.mritools.de